European Supercritical Water-Cooled Small Modular Reactor: Design and Analysis

*I. Otic[1], T. Schulenberg[1], M. Šípová[2], A. Sáez-Maderuelo[3], S. Czifrus[4], and L. Cizelj[5]

[1]Karlsruhe Institute of Technology (KIT), Eggenstein-Leopoldshafen, Germany
[2]Centrum výzkumu Řež, s.r.o. (CVŘ), Řež Husinec, Czech Republic
[3]Centro de Invest. Energéticas, Medioamb. y Tecnológicas (CIEMAT), Madrid, Spain
[4]Budapest University of Technology and Economics (BME), Budapest, Hungary
[5]Jožef Stefan Institute (JSI), Ljubljana, Slovenia

*Corresponding author. E-mail: ivan.otic@kit.edu

Abstract

This paper presents the design concept and in-depth analysis of a European Super-Critical-Water-cooled Small Modular Reactor (SCW-SMR), developed within the framework of the Joint European-Canadian-Chinese (ECC-SMART) project, aimed at advancing next-generation nuclear reactor technologies. The reactor features an innovative horizontal fuel assembly configuration with seven heat-up stages and intermediate mixing zones, specifically designed to enable passive residual heat removal through natural circulation. The horizontal core configuration generates unique natural circulation patterns in the vessel that improve heat removal efficiency during accident conditions. Key innovations include the elimination of high-pressure injection requirements through the strategic use of subcooled water inventory, the reliance on the large volume of feedwater at 280 °C as a thermal buffer, and the successful demonstration of passive decay heat removal for extended periods that exceed 72 hours. Based on extensive material testing within the ECC-SMART, the design specifies 310S stainless steel and Alloy 800H as alternative candidates for fuel cladding. Comprehensive safety analyses demonstrate the reactor's capability to manage design basis accidents, including long-term station blackout (LTSBO) and large-break loss-of-coolant accidents (LBLOCA) using primarily passive safety systems. Detailed thermal-hydraulic analyses confirm acceptable peak cladding temperatures below 625°C during normal operation and below 780°C during design-based accidents. Neutronic analyses and coupled neutronic–thermal-hydraulic simulations confirmed strongly negative reactivity coefficients and demonstrated feasibility of a two-year burnup cycle without fuel shuffling. The European SCW-SMR design is a 290 MW_{th} reactor operating at 25 MPa with core outlet temperatures of 500 °C, achieving thermal efficiency approaching 44%. The design represents a significant advancement in Generation IV reactor technology, combining the inherent simplicity of supercritical water cooling with enhanced passive safety features suitable for small modular deployment.

Keywords: SCW-SMR; supercritical water reactor; passive safety; horizontal fuel assemblies; natural circulation; core design; cladding materials; Generation IV

1 Introduction

Background and Motivation

Supercritical water-cooled reactors (SCWRs) represent one of the six Generation IV reactor concepts selected by the Generation IV International Forum (GIF) for their potential to achieve sustainability, economics, safety, and resistance to proliferation [1]. The SCWR concept takes advantage of the unique thermodynamic properties of water above its critical point (374°C and 22.1 MPa) to achieve thermal efficiencies exceeding 44%, outperforming current light water reactors (LWRs) operating at 33-35% efficiency. One of the main advantages of SCWRs compared to conventional water-cooled reactors lies in the once-through steam cycle with higher steam enthalpy at the turbine inlet, which leads to increased efficiency and reduced capital and fuel costs, see, e.g., Pioro [2]. The aim of reducing investment costs and risks, better integrability to smaller electricity grids, and the possibility of providing alternative product streams have also placed small modular reactors in the focus of recent R&D activities; see, e.g., Ingersoll and Carelli [3].

The development of SCWR Small Modular Reactor (SMR) variants addresses growing market demands for flexible, economically viable nuclear power solutions with enhanced safety features and reduced capital investment requirements. The Joint European-Canadian-Chinese development of Small Modular Reactor Technology (ECC-SMART) project [4], aims to advance SCW-SMR technology through collaborative international research addressing critical challenges in materials science, thermal-hydraulics, safety analysis, and regulatory framework development. The first design concept of a European SCW-SMR is introduced in Schulenberg and Otic [5].

European Market Context and Deployment Scenarios

According to the European SMRs Partnership report [6], the market potential of SMRs in Europe varies based on deployment scenarios:

- **Current projection**: 15 GW installed capacity by 2050 (half of the announced projects reach completion)
- **Boosted deployment**: 50 GW with EU SMR Industrial Alliance support
- **Net Zero 2050**: 100 GW for complete decarbonization of Europe's economy

SCW-SMR technology addresses specific European energy needs, including the replacement of aging coal-fired power plants, the provision of district heating for northern European cities, industrial steam supply for chemical and manufacturing processes, and the support of grid stability to increase the penetration of renewable energy.

Evolution from Previous Concepts

This paper presents the European SCW-SMR concept developed within the ECC-SMART project [4]. The design is based on extensive experience in Light Water reactor technology (LWR) and High Performance Light Water Reactor (HPLWR) project [7], incorporating lessons learned from multiple international SCWR development programs; see, e.g. Oka et al. [8], Pioro [9] and Yamaji et al. [10]. The Canadian SCWR program contributed valuable analysis and insight on pressure-tube designs and heavy water moderation, see e.g. Yetisir et al. [11], Nava-Dominguez et al. [12] while Chinese research provided analysis and design with mixed moderator concepts and two-pass flow configurations, see IAEA TECDOC-1869 [13], Nava-Dominguez et al. [14] and **?**].

Design Strategy

The primary innovation of the European SCW-SMR lies in its horizontal fuel assembly orientation with seven sequential heat-up stages and intermediate mixing zones. This configuration specifically addresses fundamental challenges identified in earlier SCWR concepts:

- Elimination of siphon effects that prevented natural circulation in three-pass vertical designs
- Reduction of the peak cladding temperatures through enhanced mixing between heat-up stages
- Promotion of passive safety through buoyancy-driven natural circulation
- Simplification of control rod mechanisms through transverse insertion

The design philosophy prioritizes passive and inherent safety features consistent with Generation IV objectives, particularly the goal of eliminating the need for offsite emergency response. This approach aligns with current regulatory requirements that favor designs which can demonstrate safety primarily through natural circulation rather than active systems.

The remainder of the paper is organized as follows: Section 2 describes the design concept of the European SCW-SMR. In section 3 an overview of thermal-hydraulic and safety analysis is presented. In section 4 an overview of reactor core design and analysis is provided. Section 5 reviews the results on materials and structural analysis. In section 6 key regulatory and licensing approach is presented. In section 7 economic considerations and main points for future development are discussed. Section 8 provides conclusions.

2 Design Concept

Before detailed analysis of the SCW-SMR design is performed, it is essential to understand the fundamental operational differences between conventional Boiling Water Reactors (BWRs) and SCWRs, as illustrated in Figure 1. In a BWR, the core operates with internal coolant recirculation. Saturated steam is separated and dried before being supplied to the turbine, while the liquid phase recirculates through a downcomer to the core inlet. Power control in the upper load range is achieved through pump speed variation, with the feedwater system controlling the liquid level inside the RPV. An SCWR, in contrast, operates without internal coolant recirculation as steam and liquid cannot be separated at supercritical pressure. The liquid coolant entering the core is continuously heated until it becomes superheated steam at the core outlet. This fundamental difference necessitates the following:

- Core power control is achieved exclusively through control rods
- Core outlet temperature control via feedwater flow rate
- Pressure control through turbine governor valve operation
- Different residual heat removal strategies

The absence of internal recirculation in SCWRs presents unique challenges for residual heat removal. While BWRs can rely on natural circulation driven by density differences between the liquid in the downcomer and steam in the core, SCWRs must establish natural circulation loops outside the Reactor Pressure Vessel (RPV) or maintain forced convection through the core. This fundamental difference drove the development of the horizontal core configuration presented in this work.

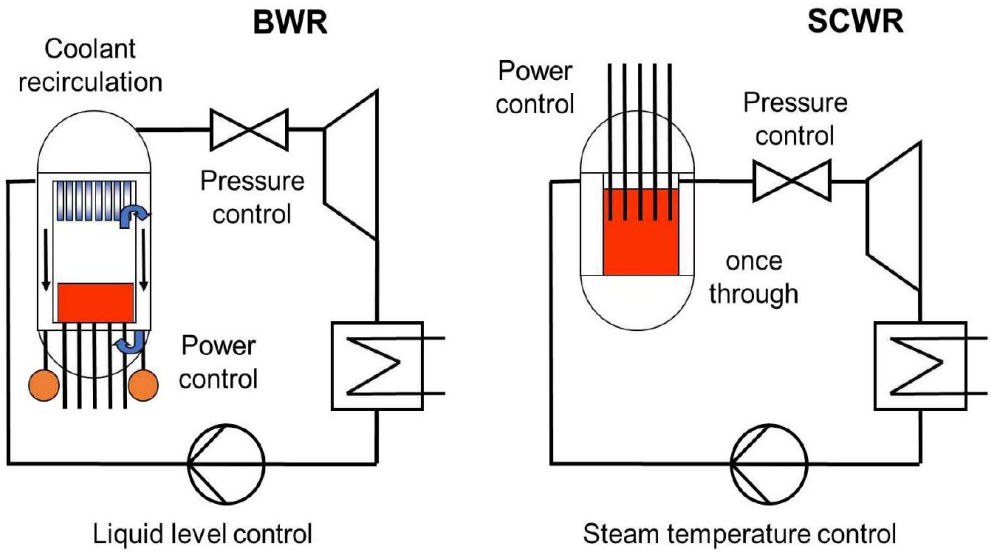

Figure 1: Generic differences between BWR and SCWR operation: BWRs employ internal coolant recirculation and liquid level control, while SCWRs use once-through flow with steam temperature control

Table 1: Main design parameters of the European SCW-SMR

Parameter	**Unit**	**Value**
Reactor Core		
Core thermal power	MW	290
Operating pressure	MPa	25
Core inlet temperature	°C	280
Core outlet temperature	°C	500
Mass flow rate	kg/s	144-150
Number of fuel assemblies	-	400
Core configuration	-	20×20 square lattice
Active fuel length per stage	m	1.68
Total core flow path	m	11.76
Peak linear power rating	kW/m	39
Reactor Pressure Vessel		
RPV inner diameter	m	4.17
RPV total height	m	8.1
Core box diameter	m	3.42
Core drum diameter	m	3.66
RPV wall material	-	20 MnMoNi 5 5
Reactivity Coefficients		
Coolant temperature coefficient	pcm/K	-16.8 ± 1.6
Moderator temperature coefficient	pcm/K	-10.6 ± 0.5
Fuel temperature coefficient	pcm/K	-1.3 ± 0.2

Reactor Configuration

The European SCW-SMR employs a Reactor Pressure Vessel (RPV) design optimized for passive safety and operational simplicity. The SCW-SMR concept has a thermal power of 290 MW, an outlet pressure of 25 MPa and a total coolant mass flow of 145 kg/s. Key design parameters are summarized in Table 1.

Fuel Assembly

The fuel assembly design is essentially taken from the HPLWR: each fuel assembly contains 40 fuel rods with helical spacers (wire wraps) to improve coolant mixing within the fuel assembly and an internal water channel (moderator box) to compensate for the insufficient moderation of the coolant. Each fuel assembly contains 40 fuel rods arranged around a central square moderator box. Detailed fuel assembly parameters are provided in Table 2.

Table 2: Fuel assembly design parameters

Parameter	**Unit**	**Value**
Fuel Pin Geometry		
Fuel rod outer diameter	mm	8.0
Fuel pellet outer diameter	mm	6.90
Fuel gas gap thickness	mm	0.05
Fuel cladding thickness	mm	0.5
Wire spacer diameter	mm	1.34
Wire spacer axial pitch	mm	200
Number of fuel rods per assembly	-	40
Fuel rod pitch	mm	9.44
Assembly Box Dimensions		
Assembly box inner width	mm	67.5
Assembly box wall thickness	mm	6.9
Assembly pitch	mm	99.3
Moderator box outer width	mm	26.9
Moderator box inner width	mm	20.5
Materials		
Fuel material	-	UO_2
Fuel enrichment	%	Variable (see below)
Fuel density	kg/m^3	11,000
Cladding material	-	310S stainless steel
Gas gap material	-	Helium
Insulation material	-	YSZ (7% Y_2O_3 in ZrO_2)

The outer assembly box, Figure 3, is designed as a sandwich with a stainless steel liner of 0.4 mm thickness on the inside, facing the hot steam, a Zircaloy structure with 2.5 mm thickness on the outside, facing the moderator, and a thermal insulation of Yttria-Stabilized-Zirconia (7% YO2 in ZrO2) with a thickness of 4 mm in between. The inner moderator box is designed similarly, with a stainless steel liner of 0.4 mm thickness on the outside, a Zircaloy structure with 0.8 mm thickness on the inside, and a thermal insulation of 2 mm thickness in between.

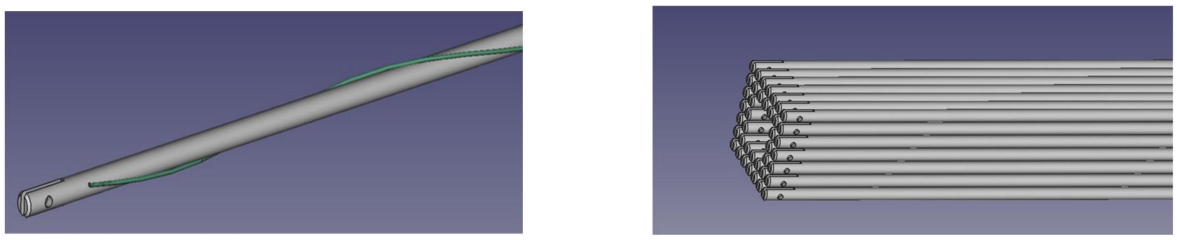

(a) Fuel rod with wire-wrapped spacer (b) Rod bundle arrangement (wires removed)

Figure 2: Fuel assembly components showing the wire-wrapped spacer configuration and rod bundle arrangement with central moderator channel

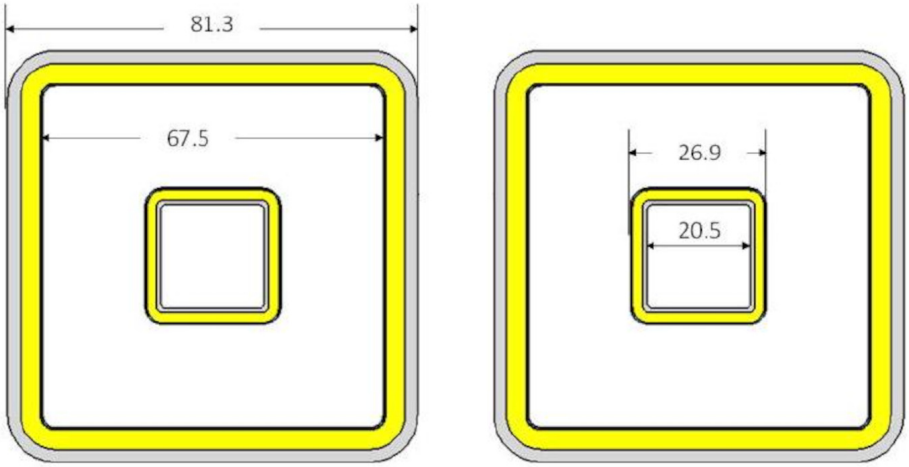

Figure 3: Assembly and moderator boxes made of Zircaloy-4 (grey) with a thermal insulation of zirconia (yellow) and a stainless steel liner (black) (dimensions in mm)

The moderator box, shown in pink in Figure 4, has a cylindrical extension on each end, which penetrates the end plates after installation. The assembly box, shown in yellow, is welded with its square end into the head end tube sheet of the reactor core. A cylindrical extension at the opposite foot end allows a sealing element such that the assembly box can freely expand when it warms up. The fuel rods are fixed in the headpiece, shown in blue in Figure 4. Vertical grid plates and horizontal bolts keep the fuel rods in place. The rods can freely expand towards the foot end when they get hot. The headpiece and assembly box are not connected. Instead, the assembly box is assumed to be welded into the tube sheet, where it remains during fuel shuffling. The headpiece can pull out the rod bundle during refuelling.

Reactor Core

Figure 5a shows a top view of the Reactor Core (RC) and its reflector. The fuel assemblies are installed horizontally with a pitch of 95 mm, leaving a gap of 21.5 mm between them for control rods or blades to be inserted from top and for a thermal insulation, which is not included here yet. The top cover of the reflector has been removed to provide a view on the three head pieces. The front plate (red) and the end plate (blue) have round openings for the moderator tubes. Suitable sealing elements like O-rings, C-rings or piston rings shall avoid ingress of the outside moderator

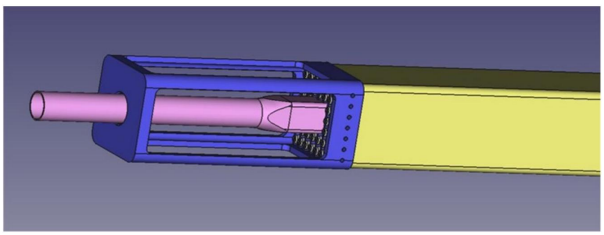

(a) Head end of the fuel assembly with head piece (blue), assembly box (yellow) and moderator box (pink)

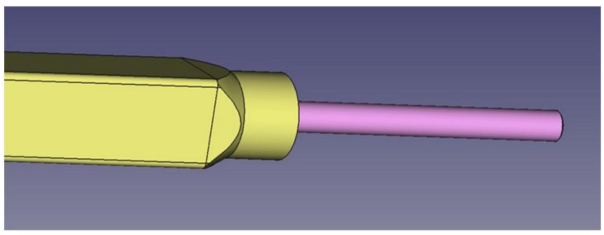

(b) Foot end of the fuel assembly with cylindrical extension to enable a C-ring, O-ring or piston ring for sealing.

Figure 4: Fuel assembly

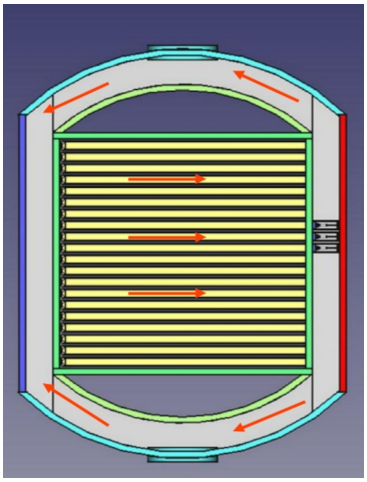

(a) Top view of the RC; top cover removed.

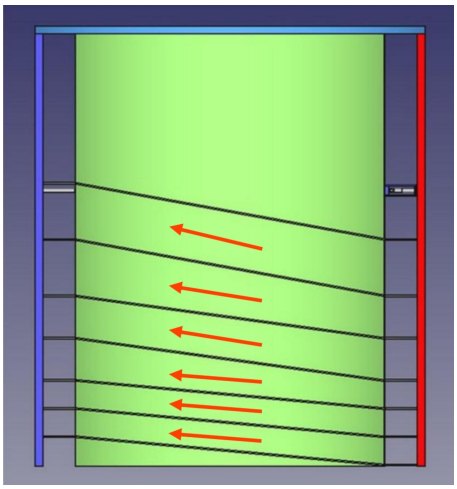

(b) Side view of the RC; outer cylinder removed.

Figure 5: Reactor core. Top and side view.

water into the internal coolant flow path. Figure 5b shows a side view of the reactor core, with the outer cylinder removed (light blue in Figure 5a), shows how the coolant coming out through the head pieces is returned via the reflector to inlets at a higher level. The first three heat-up steps at the bottom have two rows of fuel assemblies each. The warmer the coolant gets, the lower will be its density. Therefore, the next two heat-up steps need three rows of fuel assemblies each, and the last two heat-up steps have even four rows each. This way, the pressure drop in the last heat-up steps is not much higher than in the first heat-up steps.

A side view of the head end of the reactor core is shown in Figure 6a. Here, the red front plate and the outer cylinder have been removed. We can now see how the different heat-up stages are simply separated by horizontal plates welded to the tube sheet. On top of the core is a steam plenum above the reflector room, from where the superheated steam leaves via two outlet flanges. We can see these flanges in Figure 6b. The bottom and top of the reactor core are open, allowing moderator water to pass through easilly. Outside the square core box and inside the inner cylinder of the reflector is another room with moderator water, which shall help to flatten the transverse power profile, as the coolant will no longer serve as a neutron reflector once its density drops to steam-like conditions.

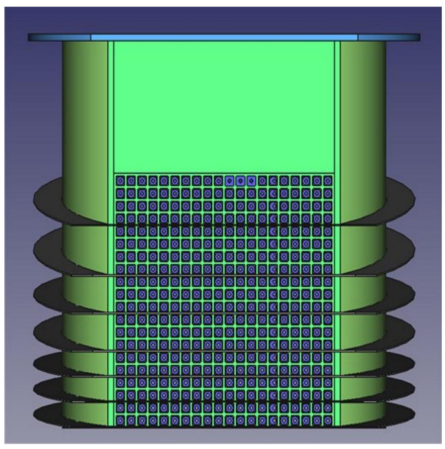

(a) Side view onto the head end of the reactor core

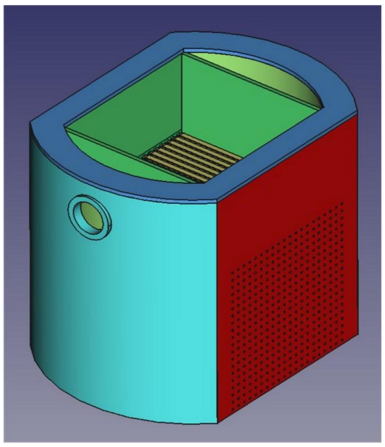

(b) Reactor core and its reflector.

Figure 6: Reactor core

Reactor Pressure Vessel

Figure 7 shows the Reactor Pressure Vessel (RPV) arrangement with the core drum suspended in the reactor flange and the horizontal core box configuration. The basic idea of this core is that the coolant enter the fuel assemblies always from the foot end side and leaves the fuel assemblies at the head end side. From there, the coolant returns back to the foot end side via the reflector. On its way back, the coolant is mixed before entering the next heat-up stage.

The cooling and the moderation are provided by the same fluid flowing multiple times through the core. In Figure 8 the vertical cross-sections of the RPV are presented, where the numbering is introduced to describe the flow path. The feedwater enters the reactor vessel at the inlet nozzles at a temperature of 280°C (1), from which the most of the fluid flows downward through the downcomer (2) into the lower plenum (3). The reactor flange contains orifices (4) that provide a fluid bypass directly to the upper plenum (5). From the lower plenum the feedwater flows upward in two parallel paths. The main part enters the core to flow through the moderator channel of the assembly (6), while the rest flows through the reflector space formed on the sides of the core (7). These paths mix again above the core (8), from where the moderator continues towards the upper plenum (9) and mixes with the bypass flow. From there, the flow turns downward towards the moderator channel inlet plenum (10) and enters the moderator boxes of all seven stages simultaneously from the side of the core. The moderator is collected in the outlet moderator plenum on the opposite side (11). Then, it continues downward, passing through two channels (12) under the core before returning to the inlet side again (13). In this region, the temperature of the water reaches approximately 310°C. From there, the primary function of the fluid is to transfer the heat through all seven stages, one after the other. The coolant first passes through the fuel assemblies of the first heat-up stage from the inlet coolant plenum (13) to the outlet (14). From there, the coolant flows through the steal stair-case structure (15) formed around the core and connecting the stage outlets with the inlet of the next stage around the reflector space - to reach the second stage inlet plenum. The stair-case flow enforces the natural convection through the core to enforce mixing in the plena and ensure the same flowing direction at all stages. Finally, when the coolant reaches the top of the core at a temperature of about 500°C, supercritical steam is collected in the annular steam dome above the core (16) to exit the reactor pressure vessel through the two hot leg nozzles (17).

All reflector components and all tube sheets may be welded together, except the front plate

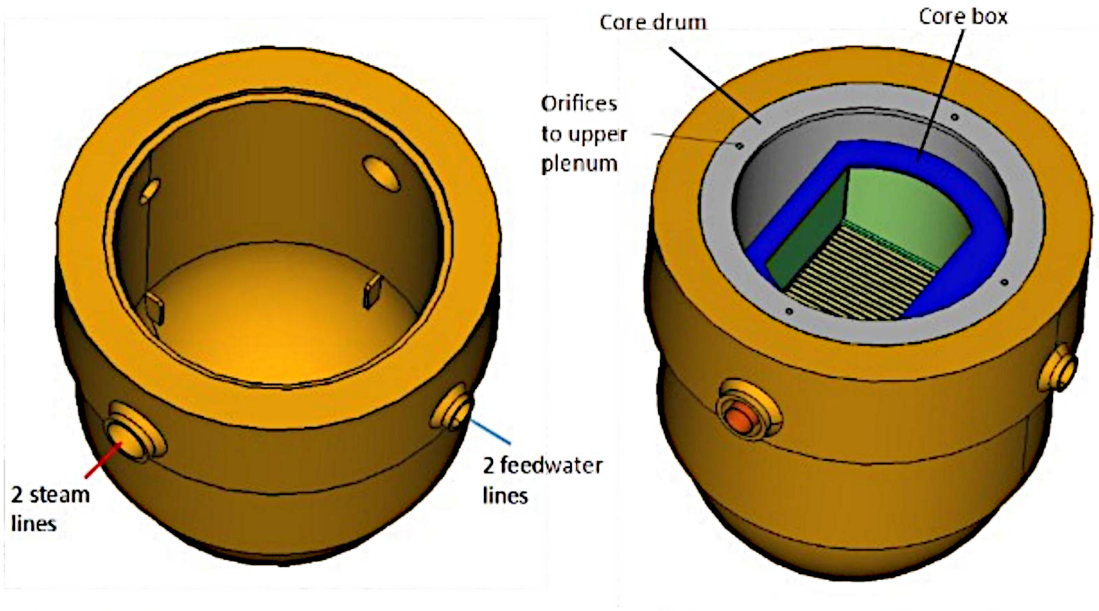

(a) Vertical section with core drum and core box

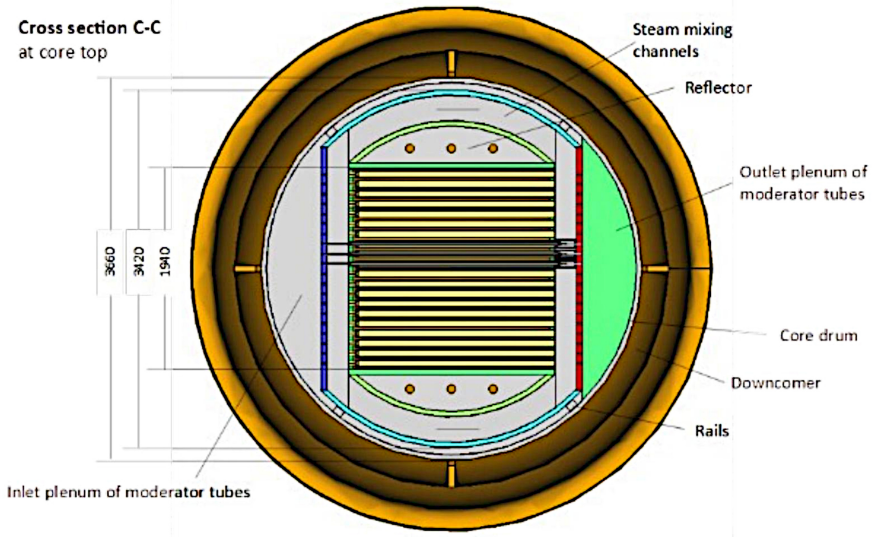

(b) Horizontal cross-section (dimensions in mm)

Figure 7: Reactor pressure vessel configuration showing the core drum (grey) suspended in the reactor flange with horizontal fuel assemblies

(red), which must be removable to exchange or shuffle fuel assemblies. The entire arrangement is mounted on a core support plate, held by a conventional core drum suspended in the reactor flange. It has a height of about 3 m, a diameter of about 3.4 m, and a weight of about 40 t. For fuel shuffling, the total arrangement shown in Figure 6b shall be removed by a crane to the spent fuel pool.

The seven-pass flow scheme represents a key innovation that enables both improved thermal performance and passive safety capabilities. Table 3 details the distribution of fuel assemblies across heat-up stages. The increasing number of parallel assemblies in higher stages compensates for decreasing coolant density, maintaining a relatively uniform pressure drop across all stages—a

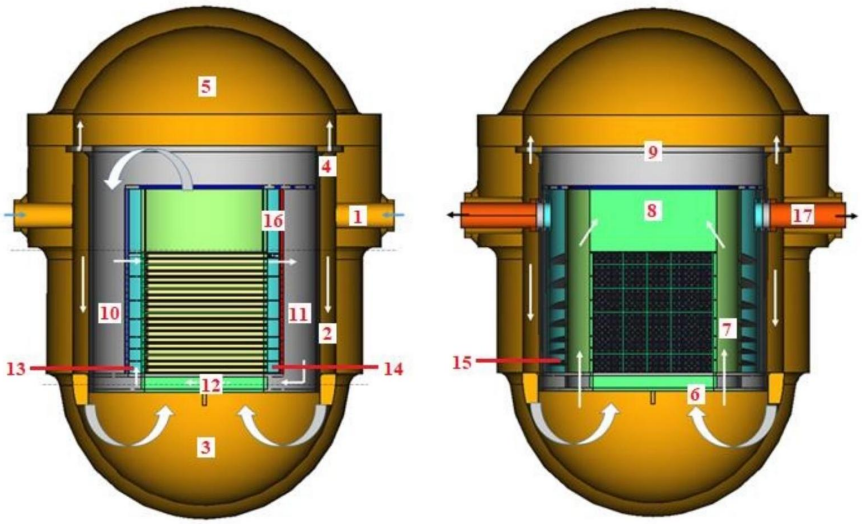

Figure 8: Vertical cross sections of the EU SCW-SMR RPV

significant improvement over previous three-pass designs.

Table 3: Distribution of fuel assemblies in heat-up stages

Heat-up Stage	FA Rows	FAs per Row	Total FAs
1	2	20	40
2	2	20	40
3	2	20	40
4	3	20	60
5	3	20	60
6	4	20	80
7	4	20	80
Total	**20**	-	**400**

Safety Systems Design

The SCW-SMR safety design follows defense-in-depth principles with an emphasis on passive and inherent features. Figure 9 illustrates the minimum set of safety systems required.
Reactor SCRAM is provided by shut-down rods falling from top into the reactor core like in a PWR. Similarly, a boron injection system is foreseen as a second, independent shut-down system, shown in yellow. Systems which are used under normal operation are shown in blue. In case of a reactor SCRAM, the turbine is tripped by the emergency stop valve at the turbine inlet and the turbine bypass valve opens, both passively by a spring, keeping a high pressure inside the RPV. The containment isolation valves stay open. The feedwater pump provides sufficient mass flow rate to cool the fuel rods as needed. In case of loss of offsite power, the containment isolation valves (CIV) are closing and the pressure relief valves (PRV) must open to avoid a pressure increase inside the RPV. Without any coolant pump, however, they may not close again but the core must

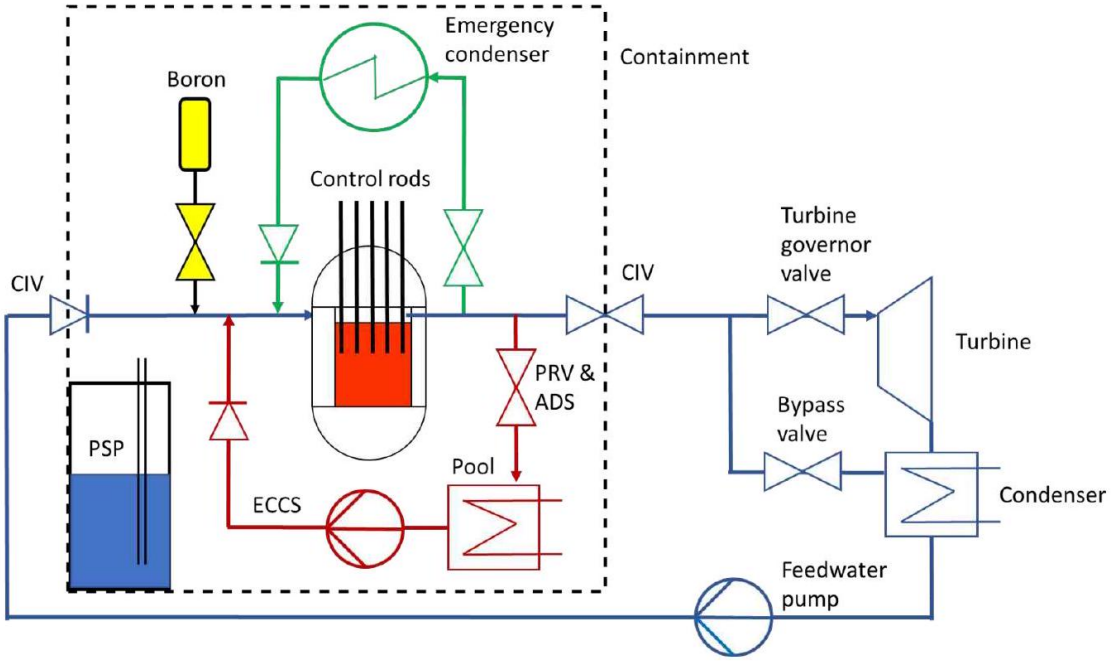

Figure 9: Minimum set of safety systems for the SCW-SMR: Systems for normal operation (blue), active safety systems (red), and passive safety systems (green)

be depressurized, at least slowly, by an automatic depressurization system (ADS) to maintain sufficient mass flow rate through the core. The released steam condenses in a cooled pool inside the containment, from where it can be pumped back into the RPV by an active emergency core cooling system (ECCS), shown in red in Figure 9.
The feedwater temperature inside the RPV is less than 310°C, and this water stays liquid until a pressure of 10 MPa is reached. If the emergency core cooling pump can be activated within this time frame, the coolant injection system will drive the coolant flow through the core and the core stays well-cooled for long term. Once the saturation pressure has been reached, the feedwater inside the RPV starts boiling. The RPV now acts as a pressurizer. The produced steam keeps the pressure high enough to drive a coolant flow through the core until the water level dropped down to the core inlet. Once the emergency core cooling pump starts injecting cold water into the RPV, however, the pressure inside drops rapidly, the core flow stops and the core overheats. It is necessary therefore to inject coolant immediately, e.g. within less than 20 s, which is quite a challenge for the diesel generators and for the pumps in case of loss of offsite power. Accumulators, as used for PWRs in their primary system, are recommended to replace the lost coolant faster and thus to gain more grace time for the ECCS.
Even more grace time for operation can be reached with a passive residual heat removal system, shown in green in Figure 9, which is favored for a small modular reactor. In case of a station black-out, the reactor SCRAM causes a turbine trip and the containment isolation valves close passively. The pressure relief valves open and they stay open to depressurize the RPV, maintaining a minimum mass flow rate through the core. Then a riser to an emergency condenser opens and condensate from the emergency condenser returns, driven by gravity, replacing the evaporated coolant. Once this passive heat removal system is working, the pressure relief valves close again. The emergency condensers are placed at an elevation of 15 to 20 m above the core to provide enough pressure head. The ultimate heat sink may be the outside atmosphere, which has an unlimited capacity, or water

pools inside the containment, which are sheltered against outside attack, but which can provide a heat sink only for about 72 hours.
In case of a loss of coolant outside the containment, the containment isolation valves are closing and the reactor core can be cooled as explained above with active or passive safety systems. In case of a loss of coolant inside the containment, pressure suppression pools inside the containment are designed with vent pipes, open at both ends like in a BWR, to limit the containment pressure. In case of a small break, the ADS is depressurizing the RPV to maintain a minimum coolant mass flow rate. Consequently, a high pressure coolant injection system is not required. Once the RPV has been depressurized, however, or in case of a large break, the lost coolant must be replaced, preferably gravity-driven, from elevated pools. All figures presented in this section are reproduced or adapted from public deliverables of the ECC-SMART project [15], [16].
Detailed description of the design concept is provided by the developers in Schulenberg and Otic [17], Schulenberg and Otic [18] and Schulenberg and Otic [5].

3 Thermal-Hydraulic and Safety Analysis

Safety analysis of the European SCW-SMR concept represents a critical component of the pre-conceptual design and analysis. The primary objective of these analyzes was to demonstrate the viability of the proposed passive safety systems and their ability to maintain core integrity during severe accident scenarios. The novel seven-stage horizontal core configuration, while advantageous for improving natural circulation, presents unique challenges for safety analysis due to its complex flow paths and reliance on passive mechanisms for accident mitigation.

Subchannel analysis

The subchannel analysis provided an evaluation of local thermal-hydraulic phenomena within fuel assemblies, enabling identification of potential hot spots and validation of flow distribution optimization and strategies. Steady-state analyses confirmed that cladding temperatures remain within design limits during normal operation and anticipated operational occurrences, providing essential data for safety assessment margins.

The analysis used two independent subchannel codes: ASSERT-PV SC, Nava-Dominguez et al. [19], developed for Canadian Pressurized Heavy Water Reactor (PHWR) applications and modified for supercritical conditions, and STAFAS Ambrosini et al. [20], developed at KIT specifically for supercritical water applications and further developed by BME Varju et al. [21]. The comparative analysis demonstrated reasonable agreement between codes, although notable differences required further investigation. Validation efforts revealed that horizontal flow stratification effects, not fully captured by either code, require additional model development. The STAFAS code particularly requires improvement to account for buoyancy-driven phenomena in horizontal channels. Figure 10 illustrates the comparative predictions, demonstrate overall agreement with the systematic differences attributed to modeling approaches for cross-flow mixing.

The key findings of the subchannel analysis include maximum cladding temperatures that remain below 625°C during normal operation, hot channel factors of 1.15 for enthalpy rise, and peak temperatures occurring at approximately 60% of heated length in stage 7. However, stage 7 also exhibits the largest discrepancy between the codes, highlighting the need for further improvements to the STAFAS code.

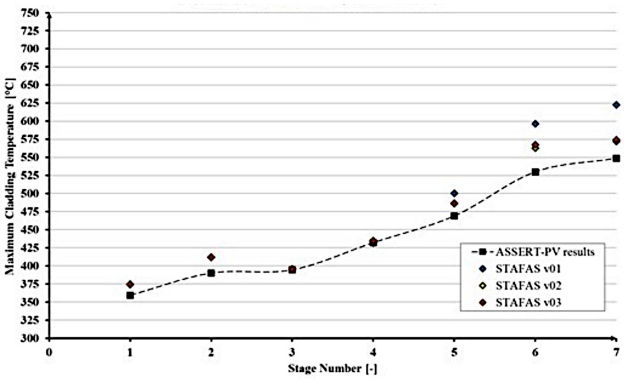

Figure 10: Comparison of maximum cladding temperature predictions by ASSERT-PV SC and STAFAS subchannel codes across seven heat-up stages

Safety analysis framework

The safety analysis framework integrates deterministic safety assessment methodologies with advanced thermal-hydraulic modeling capabilities. Two independent system codes were used to ensure validation: RELAP5 [22] and APROS [23], each providing complementary information on the progress of the accident.

The RELAP5 required substantial modifications to accommodate supercritical water properties, including the implementation of NIST property tables and modified heat transfer correlations appropriate for the supercritical regime Chaaraoui et al. [24]; Ambrosini et al. [20]; Zhao et al. [25]. The developers enhanced APROS with additional heat transfer correlations specifically validated for supercritical flows, providing improved resolution of local phenomena.

Coupled neutronic-thermal-hydraulic analysis using APROS with Serpent 2 [26] Monte Carlo code captured the dynamic feedback between the power distribution and the changes in the coolant density. This coupling revealed that negative reactivity feedback from density variations provides substantial inherent safety margins during the initial accident phase, reducing peak cladding temperatures by approximately 50 °C compared to point kinetics assumptions.

The framework establish reference experimental data base Otic et al. [27] and ecompass systematic evaluation and benchmarking of heat transfer correlations under supercritical conditions, see Kassem et al. [28]; Zhao et al. [29]; Kassem et al. [30], establishing uncertainty bands for quantification of safety margin.

The comprehensive European SCW-SMR safety assessment employed multiple computational approaches for various safety scenarios. In the following, we discuss an LTSBO scenario in which a complete loss of off-site power occurs simultaneously with the failure of all emergency diesel generators, resulting in the loss of all active cooling systems. The Long-Term Station Blackout (LTSBO) represents one of the most challenging accident scenarios for nuclear reactor design, particularly for concepts that rely on passive safety features.

Long-Term Station Blackout Analysis

The reactor protection system successfully initiates a reactor scram, but all forced circulation pumps coast down, leaving only passive mechanisms available for decay heat removal. The accident progression involves several distinct phases: initial depressurization through the opening of pressure relief valves, the establishment of natural circulation flow patterns, activation of passive heat removal systems, and long-term decay heat removal through isolation condensers. The com-

plex seven-stage core configuration presents particular challenges for the establishment of natural circulation due to multiple flow paths and the potential for flow stratification in horizontal channels.

The RELAP5 analysis demonstrated that controlled depressurization followed by passive system activation could successfully manage the LTSBO event. The analysis revealed that natural circulation patterns develop approximately 30 minutes after the initiation of the event, with stable flow rates sufficient to remove decay heat. Pressure relief valves maintain a minimum mass flow rate through the core during the depressurization phase, preventing the departure from nucleate boiling and maintaining cladding integrity, see Deliverable D3.3 Ambrosini et al. [31].

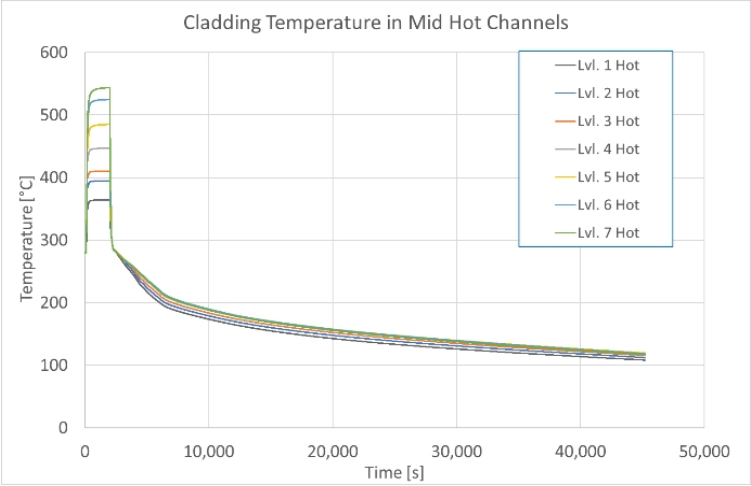

Figure 11: Transient trend of cladding temperature for the base case LTSBO scenario (RELAP5 analysis). The results show the initial temperature spike during depressurization followed by stabilization and gradual decrease as natural circulation establishes.

Figure 11 presents the transient trend of the cladding temperature for the base case LTSBO scenario at two different operating pressures. The results show that after an initial temperature increase during the early depressurization phase, the cladding temperatures stabilize and then gradually decrease as natural circulation is established. The maximum cladding temperature remains well below the design limit of 850°C throughout the transient, with peak values typically not exceeding 650°C. The comparison between operating pressures of 25 MPa and 24 MPa shows a minimal impact on the overall safety performance, demonstrating the robustness of the passive safety concept.

Sensitivity analyses examined the impact of various parameters on the progression of the accident, including the elevation of isolation condenser units, system pressure, and minor loss coefficients. The results indicated that lowering the isolation condenser units by 2 meters improved the driving forces of the natural circulation by approximately 15%, enhancing the margin of critical heat flux during the early accident phase.

The APROS simulations provided complementary insights into the LTSBO progression with enhanced resolution of local thermal-hydraulic phenomena.

Figure 12 illustrates the fluid temperatures at various locations in the vessel during the LTSBO transient. The analysis shows a short, and temporary increase in temperatures at the beginning of the transient as a result of the quick stop of feedwater injection, with the exception of the first stage where the peak is slightly above 300 °C. After this initial spike, the temperatures show continuous cooling, stabilizing around 160-180 °C after 12 hours, representing a stable long-term condition.

Figure 13 presents the detailed cladding temperatures at different core locations in all seven

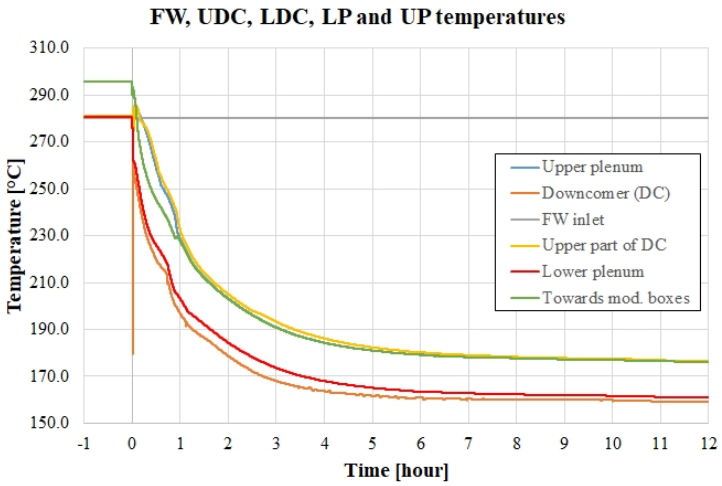

Figure 12: Fluid temperatures at various locations in the vessel during LTSBO (APROS analysis). The figure shows the initial temperature spike of 10-20°C followed by continuous cooling, stabilizing around 160-180°C after 12 hours.

stages. The results demonstrate similar characteristics with a short temporary jump of 30-40°C at the beginning followed by continuous cooling. Most importantly, the cladding temperatures show no sign of deterioration or dry-out owing to the rapid start of the depressurization blow-down and the level of cooling maintained by the passive system. The spatial distribution of the temperatures confirms that the seven-stage design effectively manages heat removal in all core regions.

Figure 14 shows the maximum temperatures of the coolant, cladding and central fuel for each of the seven stages. This comprehensive view demonstrates that all stages maintain temperatures well below safety limits, with Stage 7 (the outlet stage) experiencing the highest temperatures due to accumulated enthalpy rise. The results confirm that even in the hottest locations, significant safety margins are maintained throughout the transient, with fuel centerline temperatures remaining well below 800°C and cladding temperatures staying well below the design limit of 850°C.

Several other scenarios were also analyzed, such as, for example, the Large-Break Loss-of-Coolant Accident (LBLOCA). Cold-leg LBLOCA presents the most challenging rapid depressurization scenario. A double-ended guillotine break of the 280°C inlet line was analyzed.

Main results can be summarized as:

- Hot-leg blowdown strategy maintains positive core flow
- Subcooled water inventory prevents immediate core uncovering
- Peak cladding temperature reaches 780°C at 25 seconds
- Accumulator injection provides adequate core cooling
- No credit taken for active ECCS pumps

The coupled neutronic-thermal-hydraulic approach (APROS+Serpent) captures the feedback mechanisms between power distribution and coolant density changes, essential for accurate steady-state and transient predictions. These analyses, documented in Varju et al. [32, 33, 34, 21] and Ambrosini et al. [20]; Zhao et al. [25], validated the core design parameters and operational limits. Table 4 summarizes some of the results of the APROS-Serpent analysis evaluated for small variations of the core flow rate and vessel inlet temperature.

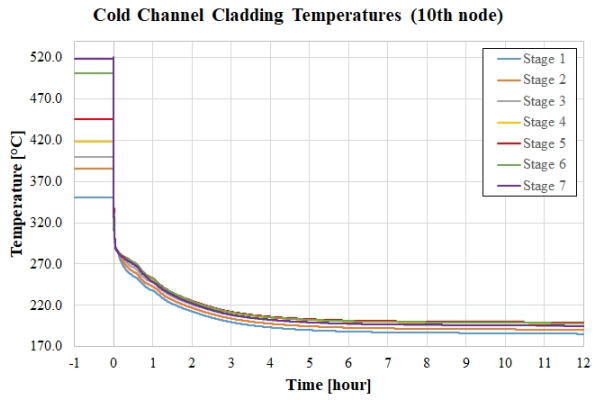

(a) Stages 1-3

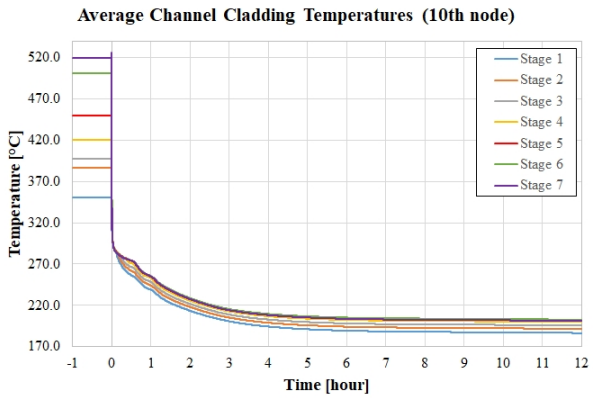

(b) Stages 4-5

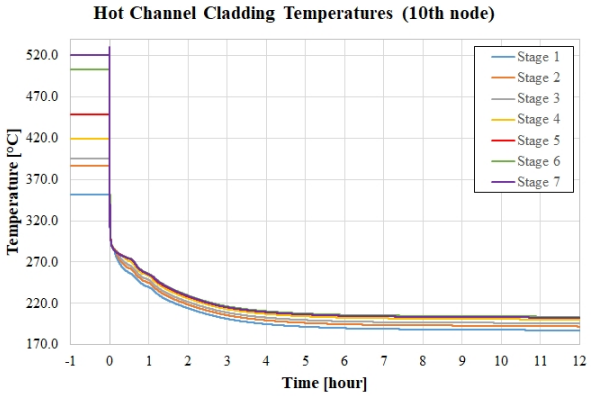

(c) Stages 6-7

Figure 13: Cladding temperatures at different core stages during LTSBO (Apros analysis). The results demonstrate a short temporary jump of ∼40 °C at the beginning followed by continuous cooling, with no signs of deterioration or dry-out.

Table 4: System thermal-hydraulic parameters from APROS-Serpent analysis

Parameter	**Unit**	**Model v1**	**Model v2**	**Model v3**
Core flow rate	kg/s	145.0	150.1	145.0
Vessel inlet pressure	MPa	25.50	25.92	25.55
Vessel outlet temperature	°C	518.1	499.4	518.3
Lower plenum temperature	°C	280.8	280.6	280.8
Upper plenum temperature	°C	297.2	295.8	298.4
Moderator inlet temperature	°C	297.5	296.1	298.7
Moderator outlet temperature	°C	320.4	316.9	321.8
Steam plenum temperature	°C	519.4	500.6	519.6

Unique Phenomena in Horizontal Configuration

Multi-Loop Natural Circulation

The horizontal core configuration generates complex but robust circulation patterns during accidents that provide multiple redundant heat removal paths.

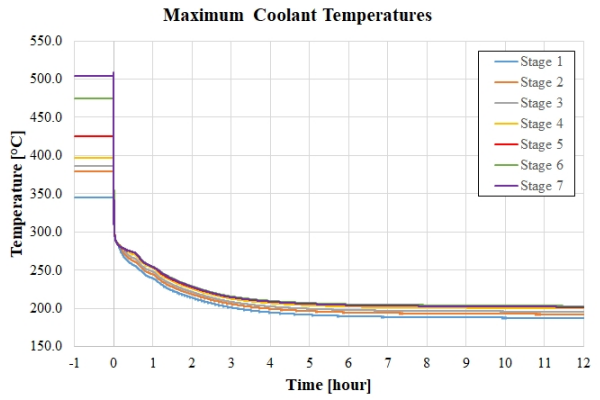

(a) Coolant temperatures

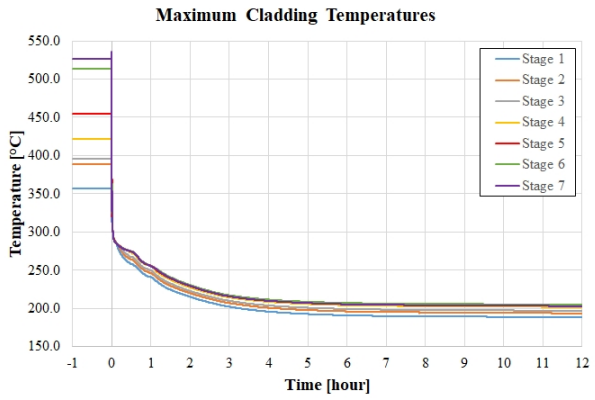

(b) Cladding temperatures

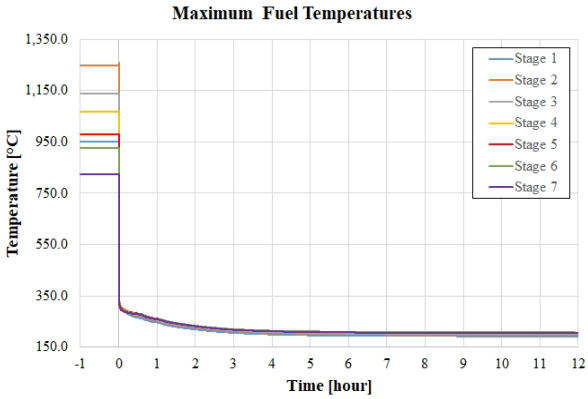

(c) Fuel centerline temperatures

Figure 14: Maximum coolant, cladding, and central fuel temperatures of the stages during LTSBO (APROS analysis). All stages maintain temperatures well below safety limits, with Stage 7 experiencing the highest temperatures due to accumulated enthalpy rise.

- **Primary circulation:** Core to isolation condensers via upper plenum serves as the dominant heat removal mode, driven by the density difference between the hot fluid in the core and the cooled fluid returning from the condensers
- **Inter-stage circulation:** Between adjacent heat-up stages through mixing channels, equalizing temperatures and preventing isolated hot regions
- **Intra-assembly circulation:** Within horizontal assemblies due to density stratification, creating local convection cells that enhance heat transfer
- **Reflector circulation:** Enhanced mixing in radial reflector regions, providing additional flow paths and thermal capacity

These interconnected loops provide redundant heat removal paths and prevent local stagnation zones that could cause fuel damage. The combination of controlled depressurization, passive heat removal through isolation condensers, and emergency coolant injection from passive accumulators provides defense-in-depth against core damage. The analyses confirmed that the cladding temperatures remain well below the design limits in all scenarios analyzed, with peak temperatures typically not exceeding 650°C compared to the design limit of 850°C.

Natural circulation proves to be a robust heat removal mechanism in the seven-stage core configuration, despite initial concerns about the complexity of the flow paths. The horizontal channel arrangement actually enhances the stability of the natural circulation by promoting flow mixing between stages and preventing the formation of stagnant regions. The analyses revealed that natural circulation mass flow rates of 8-12% of nominal flow can be sustained and sufficient to remove decay heat even several days into the accident.

Comparative Analysis with Other SCW-SMR Concepts

Table 5 compares the safety analysis results of the three SCW-SMR concepts developed within ECC-SMART, providing context for the performance characteristics of the European design, see [16]. The comparison encompasses both the design basis parameters and the accident response metrics, highlighting the advantages of the horizontal fuel assembly configuration.

Table 5: Comparison of safety analysis results for ECC-SMART reactor concepts

Parameter	**EU SCW-SMR (Horizontal)**	**Canadian SCW-SMR**	**Chinese CSR-150**
Design Basis			
Thermal Power (MWth)	290	300	150
Core Configuration	RPV, Horizontal	Pressure Tube	RPV, Vertical
Moderator	H_2O	D_2O	H_2O/ZrH
Flow Passes	7	1	2
LOCA Results			
PCT in cold-leg LOCA (°C)	780	1003	850
MFT in cold-leg LOCA (°C)	1420	1523	1450
Time to peak (s)	25	35	30
LTSBO Results			
PCT in LTSBO (°C)	680	750	710
Natural circulation capability	Enhanced	Limited	Moderate
Time to establish NC (s)	200	> 600	400
Safety Features			
High-pressure injection	Not required	Required	Required
Passive safety credit	Full	Partial	Partial
Grace time for operator action	> 30 min	< 10 min	< 20 min

The horizontal configuration demonstrates several distinct advantages: lower peak cladding temperatures in all scenarios analyzed, faster establishment of natural circulation, elimination of high-pressure injection requirements, and extended grace time for operator intervention. These improvements result from the fundamental design philosophy of ensuring all flow paths are horizontal or upward, eliminating siphon effects that plagued earlier SCWR concepts.

Design Optimization Insights

The safety analyses provided valuable insights for design optimization, particularly regarding the placement and sizing of passive safety components. Sensitivity studies demonstrated that the elevation difference between the core and isolation condensers significantly impacts natural circulation

performance, with optimal configurations providing elevation differences of 15-20 meters. The analyses also revealed the importance of flow orificing to ensure appropriate flow distribution during normal operation and accident conditions, preventing local hot spots that could challenge fuel integrity, as documented in Deliverable D3.3 Ambrosini et al. [31].

The requirement for vessel reflooding from accumulators or other water sources after several hours highlights the need for diverse passive injection systems. Although the initial accumulator inventory proves sufficient for the early accident phase, long-term cooling requires additional passive water sources or eventual operator intervention to establish alternative injection paths. This finding has led to design modifications that incorporate gravity-driven cooling tanks at higher elevations to provide an extended passive injection capability, as detailed in Ambrosini et al. [31]; Varju et al. [21].

Validation and Uncertainty Considerations

The safety analysis results benefit from the use of independent codes, providing increased confidence in the conclusions. The general agreement between the RELAP5 and APROS predictions for key safety parameters, despite the different modeling approaches and numerical schemes, validates the fundamental understanding of accident phenomenology. Differences in specific predictions, typically within 10-15% for temperatures and flow rates, fall within the expected uncertainty bands and do not affect the overall safety conclusions. The comprehensive safety analyses performed for the European SCW-SMR concept demonstrate the feasibility of achieving adequate safety performance through passive systems alone. Further detailed thermal-hydraulic and safety analyses are provided in the ECC-SMART Consortium deliverables [16], including additional accident scenarios, sensitivity studies, code validation exercises and benchmarking together with experimental and fundamental studies that support the conclusions presented here. Numerous Computational Fluid Dynamics (CFD) studies, representing significant contributions to the understanding of supercritical water flows, were performed within the ECC-SMART framework [35; 36; 37; 38]; a detailed discussion of these results is beyond the scope of this paper.

However, important areas of uncertainty remain, particularly with respect to heat transfer correlations for supercritical water under low-flow conditions and the potential for flow instabilities in horizontal channels during transients. These uncertainties were addressed in the ECC-SMART through conservative modeling assumptions and the application of appropriate safety margins, but require further detailed analysis in the future. All figures presented in this section are reproduced or adapted from public deliverables of the ECC-SMART project [15], [16].

4 Reactor Physics

Neutronics Modelling

Neutronic calculations for core development and reactivity feedback coefficients were executed primarily with the Serpent 2 Monte Carlo particle transport code (version 2.1.31), Leppänen et al. [39]. In addition, examinations encompassing in-assembly power distribution, burnup calculations, and burnable poisons were conducted with MCNP 6.2, Werner et al. [40], and OpenMC 0.12, Romano et al. [41]. The selection of neutronic codes utilized in the framework of this project and their comparison were based on the FQT fuel qualification test benchmark [42].
Initially, core development progressed alongside two aspects. First, the power distribution was shaped both vertically, in adherence to the MLHR profile, and horizontally, to decrease power

peaking. Second, the reserve reactivity of the system was increased to reach a burnup cycle length of at least two years without fuel shuffling. The highlights of this process, presented in detail in Deliverable 4.3 and in Antók et al. [43], were the following:

- The structure and materials of the fuel assembly were updated to reduce neutron absorption and enhance resistance against high thermal loads and corrosion. The assembly and moderator box walls utilize yttria stabilized tetragonal zirconia polycrystals (YTZP) as insulation between two metal layers: a Zircaloy-4 liner faces the colder moderator region, whereas an SS 310 S liner faces the coolant region with the fuel pin lattice.
- The fuel assembly gap width and the moderator temperature were examined to understand their effects on reserve reactivity, vertical power distribution, and safety (possible cases of overmoderation). Finally, an assembly gap width of 18 mm and a uniform moderator temperature of 550 K (277°C) were adopted.
- The enrichment map of the core was manipulated to reach the reserve reactivity necessary for a two-year burnup cycle, while trying to adhere to the originally constructed MLHR profile. Three assembly-averaged enrichment values (5.0%, 7.4%, and 10.0%) were implemented, resulting in an average core enrichment of 6.49%. The improved model yielded a BoC k_{eff} of 1.24239 ± 0.00007. The enrichment map and core power distribution are presented in Figure 15, while the MLHR profile can be observed in Figure 16. According to a burnup examination, this system is capable of a burnup cycle length of approximately 26 months without fuel shuffling.

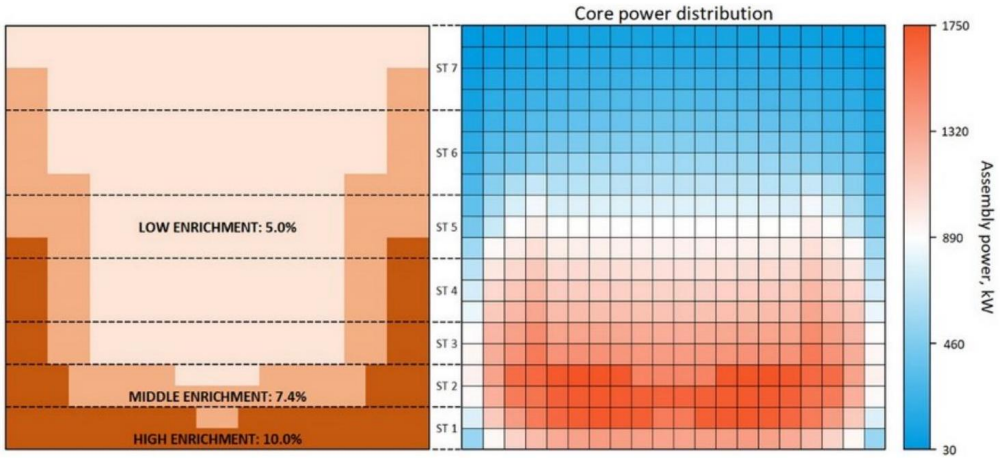

Figure 15: Improved enrichment map and the resulting core power distribution

The coolant, moderator, and fuel temperature coefficients were also determined for the improved core. The calculation method is summarized in Deliverable 4.2. The results for this core version are presented in Table 6 and Antók et al. [43].

Values are presented in pcm/K with a $\pm 2\sigma$ uncertainty.

The core model was utilized to conduct coupled neutronic-thermal-hydraulic examinations with Serpent and APROS, facilitating further model improvements. The model was updated to differentiate between cold, average, and hot assemblies in every heat-up stage and to incorporate the detailed coolant, moderator, and fuel temperature and density profiles provided. Due to the

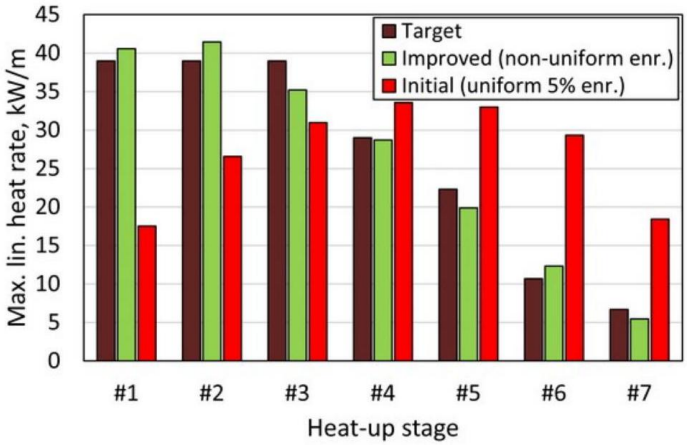

Figure 16: MLHR profile of the improved model compared to the target profile and to the initial model

Table 6: Reactivity feedback coefficients of the improved model

Coefficients	Value
Moderator temperature coefficient (inner moderator)	$-2.20(\pm 0.14)$
Moderator temperature coefficient (outer moderator)	$-3.15(\pm 0.58)$
Moderator temperature coefficient	$-5.48(\pm 0.42)$
Coolant temperature coefficient	$-23.11(\pm 0.68)$
Doppler temperature coefficient	$-1.28(\pm 0.05)$

available thermal-hydraulic feedback, the core model no longer depends on the target MLHR profile, as it now relies on the calculated (peak) temperatures. The coupling methodology, models and results are presented in the ECC-SMART Deliverable 3.3 Ambrosini et al. [31]. The final enrichment map and power distribution can be observed in Figure 17.

A study was also performed to identify possible strategies at the assembly level to reduce the reactivity inventory and homogenize the power distribution of the fuel pins. To accomplish that, the use of burnable absorbers and an appropriate enrichment zoning was investigated (Giusti [44]). A simplified analytical model was derived to estimate the effect of different lumped burnable absorbers placed inside the fuel assembly. To confirm the analytical results, Monte Carlo simulations with the OpenMC code were performed on a few selected cases. The use of 24 B_4C rods with a radius of 0.35 mm, almost uniformly distributed inside the outer yttria insulator, proved to be effective in order to reduce the multiplication factor from the value of 1.32 (no absorbers) to the value of 1.11 and to keep it quite constant up to a burnup of about 25.0 MWd/kg. Although a uniform enrichment of 7.5% would allow for an assembly burnup cycle as long as 885.0 days, the pin-power distribution is quite uneven and produces a pin-power peaking factor of 1.32 at the beginning of the cycle. Despite the natural flattening of the assembly power distribution with the fuel burnup, the pin-power peaking factor remains too high for a large fraction of the burnup cycle. Adopting six different enrichments that range from 5.3% to 8.7% while keeping the assembly average value at 7.5%, the pin-power peaking factor at BoC can be reduced to a value as low as 1.03, being almost constant through the entire burnup cycle.

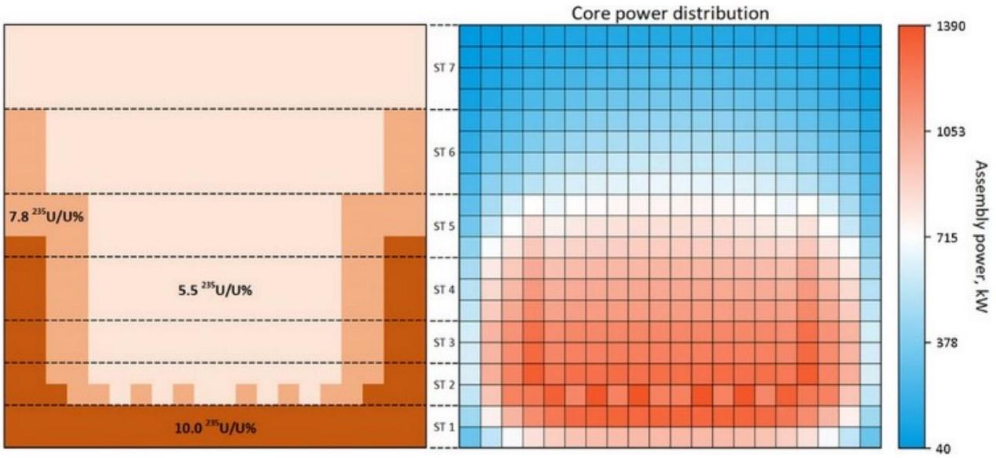

Figure 17: Coupled UO_2 core enrichment map and the resulting core power distribution Varju et al. [33]

.

The single-assembly burnable absorber study was followed by the application of the knowledge acquired regarding the burnable absorbers to the entire reactor core. After the coupled neutronic–thermal-hydraulic improvements, the UO_2 core can meet the " 2-year cycle without shuffling" objective, but it does so with very high excess reactivity at the beginning of cycle (BoC): the optimized full-core burnup run starts at $k_{\text{eff}} = 1.24965$, and even after 730 days it is still $k_{\text{eff}} = 1.02998$. The BA choice for the full-core model is motivated by the comparative fuel-assembly study (Giusti [44]) To quantify the impact in the actual coupled full-core model, a set of burnup calculations were run with 0, 8, 12, 16, 20, and 24 absorber rods per assembly, uniformly distributed around the insulation. The rod radius is fixed at 0.3 mm, so the total absorber volume changes with rod count.

With 24 rods the BoC k_{eff} drops to 1.06598, but the core becomes subcritical before the end of the second year in the full-core setting. With 20 rods the BoC k_{eff} becomes 1.08999 and remains slightly above unity after two years: 1.00146. It is concluded that this configuration best meets the design target: ∼2-year cycle without refueling/shuffling, while also giving a smoother, more acceptable reactivity curve. Therefore, the uniform embedding of approximately 20 small B_4C rods per assembly in the insulation in all of the fuel assemblies of a full core model seems sufficient to reduce the initial excess reactivity without sacrificing the intended two-year cycle.

The achieved core with a reduced BoC reserve reactivity is a great candidate for the design of the reactivity control system.

Reactivity Control System

The reactivity control system provides the means for detecting and controlling reactivity and, at least partially, neutron flux distributions. This system makes it possible to maintain reactor power for a larger timescale such as the burnup cycle. The reactivity control mechanisms, on the other hand, also limit the positive reactivity insertion rate to prevent prompt criticality and meet fuel acceptance criteria during transients.

Because of the use of supercritical water technology, boric acid cannot be used in SCW-SMR as a means of reactivity control. Without boric acid, long-term control is expected to be achieved

with burnable absorbers, along with the very slow motion of some (batches) of the control elements. The former solution could be provided by various materials and in various forms. The SCW-SMR concept has a horizontal core layout with vertical control elements moving in the gaps (see below). Therefore, the internals of the fuel assembly do not contain guide tubes for the control elements, so the use of separate burnable absorber rods as a solution would not be practical. Based on preliminary calculations, besides the application of burnable absorbers, the following concept appears to be feasible.

Movable control elements would ensure prompt reactivity control and rapid reactor shutdown. In the case of the SCW-SMR, due to the horizontal layout, it is impossible to maneuver inside the assemblies, so the absorber elements can be placed only in the narrow gap between the assemblies, which does not allow elements to be thicker than 1 cm .

The current preliminary design of the control system is to accommodate 40 control elements, 18a, with a length of 200 cm, each consisting of 15 control rods placed side by side and welded together, 18b. This type of control element design is commonly used in BWR reactors. The outer diameter of each rod is 1 cm , the wall thickness is 1 mm , the wall material is stainless steel 310S , and it contains B_4C absorber (with 80% B^{10} isotope).

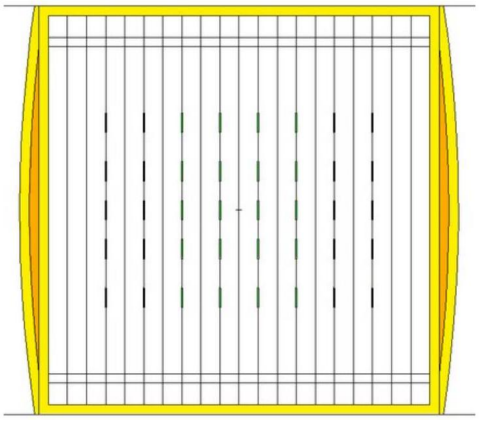

(a) Reactivity control elements in the SCW-SMR core (top view)

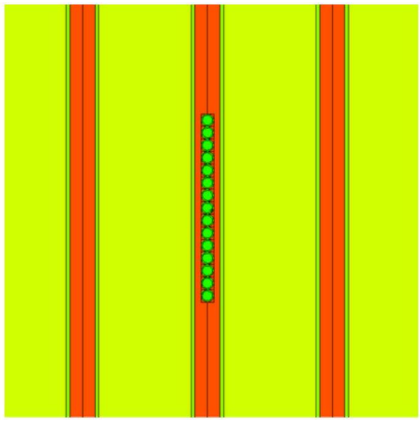

(b) One control element between the fuel assemblies, consisting of 15 control rods

Figure 18: Reactivity control elements

From a technical point of view, the control element drives have a dual function: to provide the analog intervention necessary for power control and, in a safety protection situation, to provide the necessary negative reactivity instantaneously and irreversibly. A base requirement is that the system must also be able to perform its safety protection function passively without an external power source.

In the SCW-SMR reactor concept, the control elements and their drives must operate under high system pressures. This almost completely excludes the possibility of electromechanical movement due to leakage, so the movement is planned to be based on the hydraulic principle, as in BWRs.

One of the main objectives in designing the control system was to ensure that the large initial reactivity reserve, which can provide a cycle length of at least two years, could be adequately managed under all operating and accident conditions throughout the burnup cycle. The shutdown margin, one of the most important criteria, was also examined in the analysis. According to this criterion, the system must be able to reduce the multiplication factor to at least 0.98 at all times, even when the most valuable control rod is lost. Based on the calculations performed, the proposed

preliminary system design meets this requirement both at nominal operating temperatures and at lower design temperatures.

It must be emphasized that the concept for the reactivity control system presented above is at a preliminary stage and that much research is still needed to be carried out on this topic regarding many areas, such as reactor physics, engineering feasibility, thermal-hydraulic effects, and economics.

5 Materials and Structural Considerations

Material Selection

Material selection is a key aspect of reactor design, but it becomes critically important in a horizontal core configuration. Unlike vertical geometries, where gravity assists in clearing spalled oxides or debris away from the active zone into lower plenums, horizontal channels lack this natural clearing mechanism. In this configuration, any oxide detachment (spallation) leads to debris accumulation at the bottom of the coolant channel.

This accumulation is particularly detrimental as it creates thermal barriers (causing local hotspots) and increases hydraulic resistance, which directly jeopardizes the natural circulation flow required for passive safety. Ensuring the integrity of the fuel cladding is mandatory, not only to maintain the reactor's thermal-hydraulic performance but also because the fuel cladding serves as the primary safety barrier against fission product release. For these reasons, studying the corrosion behavior of these materials under simulated operating conditions, as well as the composition and stability of their oxide layers, is a key aspect of the evaluation process.

Therefore, within the ECC-SMART project, the selection process prioritized materials with superior oxide adherence and mechanical stability. Table 7 shows the main materials considered for the European SCW-SMR.

Table 7: Primary materials selection for EU SCW-SMR

Component	**Material**	**Max. Temperature (°C)**
Fuel cladding	310S stainless steel/Alloy 800H	625
Assembly box inner liner	310S stainless steel	520
Assembly box structure	Zircaloy-4	320
Moderator box structure	Zircaloy-4	320
Thermal insulation	YSZ (7% Y_2O_3 in ZrO_2)	520
RPV	20 MnMoNi 5 5	280
Core support structures	316L stainless steel	320
Control rod cladding	Inconel 625	500

Regarding fuel cladding material selection, several key criteria must be considered, including resistance to general and stress corrosion cracking (SCC) at high temperatures; long-term microstructural stability; compatibility with the coolant water chemistry; resistance to irradiation-induced degradation; and mechanical strength at elevated temperatures, as shown in Table 7.

Zirconium alloys, such as Zircaloy-4 and Zirlo, are extensively used as fuel cladding materials in light water reactors (LWRs) due to their acceptable mechanical properties, corrosion resistance, and, most importantly, their very low neutron absorption cross-section, which is a critical factor for in-core material selection. However, the main drawback of zirconium alloys is their poor oxidation

resistance above 450°C in supercritical water (SCW), as reported by Cox [45]. This temperature limitation disqualifies them for SCW reactors.

One alternative explored was applying protective coatings to Zr-based cladding, using materials resistant to SCW corrosion. Recent research from Canadian Nuclear Laboratories (CNL) investigated the corrosion behavior of Zr-2.5Nb alloys coated with Cr, Khumsa-Ang et al. [46]. The main findings showed that, after only 1,150 hours at 500°C, oxide layers of approximately 3 µm formed. Under dual-beam irradiation, these layers underwent severe degradation, with corrosion rates up to 17 times higher. Additionally, coating delamination and substrate attack were observed. These results led to the conclusion that zirconium alloys, even when coated with protective layers such as chromium, are not viable candidates for SCW-SMR cladding as also indicated previously by Cook et al. [47]. Much of the research on alternative materials to zirconium dates back more than 50 years to the superheated steam reactor designs. Among the evaluated candidates, ferritic steels stood out for their high swelling resistance, but their poor corrosion resistance in SCW combined with mechanical properties that degrade significantly above 650°C, provides further justification for their exclusion from the candidate list Allen et al. [48].

Nickel-based alloys were also investigated. These materials have shown excellent performance in pressurized water reactors (PWRs). For instance, Alloy 690 TT has demonstrated excellent in-service corrosion resistance since its installation in the late 1980s, which led to its consideration for SCWR applications Payet et al. [49]. However, their use as fuel cladding materials is not optimal due to their poor neutron transparency, up to 15 times worse than zirconium, along with helium production under irradiation, which contributes to swelling and embrittlement Nuclear Energy Agency (NEA). Committee on the Safety of Nuclear Installations [50]. Furthermore, their high cost poses additional limitations for large-scale application.

Stainless steels, especially austenitic grades such as 304, 316, 310, and 800H, are key candidate materials for SCW-SMR applications due to their high-temperature strength, corrosion resistance, ease of fabrication and welding, and well-established operational performance in LWRs. Stainless steel 316L exhibited significant degradation of the protective oxide layer at 500–550°C in SCW; see Behnamian et al. [51]. Type 310S, with higher Cr and Ni content and proven performance in fossil supercritical boilers, shows improved oxidation resistance but remains susceptible to stress corrosion cracking (SCC) in high-oxygen environments. Alloy 800H, which holds ASME Section III qualification for nuclear service up to 760°C and is widely used in steam generators, represents an intermediate option whose performance is highly dependent on environmental conditions. Based on their favorable behavior and optimal overall properties, Alloys 800H and 310S were selected as the primary reference materials in the ECC-SMART project [52]. However, both alloys may undergo stress corrosion cracking, lose ductility due to irradiation, and exhibit low neutron transparency. Irradiation with fast neutrons may result in high swelling rates. Overall, more comprehensive and long-term studies are necessary to thoroughly understand their behavior in supercritical water environments.

Additionally, advanced alloys such as Alumina-Forming Austenitic (AFA) alloys are promising materials due to their improved corrosion resistance resulting from the formation of a stable alumina (Al_2O_3) layer when the aluminum content is approximately 2.05–5.03 wt%. The alumina-based oxide layer offers superior protection compared to Cr_2O_3-forming alloys, mitigating chromium evaporation at high temperatures and downstream deposition. However, challenges remain, including maintaining the desired matrix structure with aluminum additions and improving our understanding of their behavior under simulated SCWR operating conditions. Specifically, an alumina-forming austenitic alloy based on 310S stainless steel was evaluated in this project under the same conditions as the reference alloys 800H and 310S.

This section focuses primarily on the results obtained for the two main candidate alloys, Alloy

800H and austenitic stainless steel 310S. A brief summary of the key findings for the AFA alloy, which was tested under the same conditions in both as-received and heat-treated states, is also provided. The heat treatment was performed at 850°C for 50 h to produce a more protective alumina layer on the surface of the material. Despite their advantages and known limitations, these materials exhibit the most clearly favorable properties among candidate materials for use as fuel cladding in the SCW-SMR. However, existing corrosion data in supercritical water environments remain limited. To progress toward their qualification for SCW-SMR and SCWR designs, it is essential to significantly expand the available dataset and extend exposure times to longer durations, on the order of thousands of hours. This would help refine the prediction tools, given that the expected fuel cladding lifetime in the SCW-SMR is approximately 30,000 h. Furthermore, a better understanding of their corrosion behavior under neutron irradiation, as well as the effects of fluctuations in the physicochemical properties of water near the critical point, is necessary. The reference chemical composition of the three studied materials is presented in Table 8.

Table 8: Chemical composition of candidate cladding materials (wt%)

Alloy	Fe	Cr	Ni	Mn	Si	C	Al	Ti
310S	Bal	24.5–25.5	19–22	2.0	<1.0	<0.08	–	–
800H	39.5 min	19–23	30–35	<1.5	<1.0	0.05–0.10	0.15–0.60	0.15–0.60
AFA	Bal	20–25	20–25	<2.0	<0.5	<0.1	3.5–5.0	–

As part of ECC-SMART, the effect of geometry on alloy performance was also considered a key study point. For this reason, both steel 310S and Alloy 800H were evaluated using samples manufactured from tubes, in order to replicate as closely as possible the behavior of the real reactor component, within the limitations of the consortium's experimental facilities. The geometry of 310S/800H samples, used for both corrosion and Slow Strain Rate Tensile (SSRT) tests, is shown in Figure 19.

Corrosion Behaviour in Supercritical Water

This section focuses primarily on the results obtained for the two main candidate alloys, Alloy 800H and austenitic stainless steel 310S. In addition, a brief summary of the key findings for the alumina-forming austenitic alloy based on 310S (AFA) is provided. The test conditions were: 500°C and 380°C; 23 MPa and 25 MPa; with an oxygen concentration of 150 ppb. The selection of 380°C was aimed at investigating the corrosion behavior near the critical and pseudo-critical points at 23 and 25 MPa, respectively. According to studies by Liu et al. [53] and Hayward et al. [54], corrosion rates tend to increase near the critical point. Moreover, this operational window has not been extensively explored in the literature, which justifies its inclusion in the current work.

The corrosion tests were conducted over exposure durations of 1,000 hours and 7,000 hours (with several intermediate stops). Additionally, an extrapolation of oxide layer thickness over time was performed to estimate its growth up to 30,000 hours, which corresponds approximately to the expected operational lifetime of the fuel for the pre-concept of the SCW-SMR.

In addition to corrosion testing, accident simulation tests were conducted under Loss of Coolant Accident (LOCA) conditions, based on the corresponding NRC standard [55]. These tests were carried out at temperatures up to 1200°C, under atmospheric pressure for approximately 8 hours, simulating the thermal exposure conditions expected during a severe accident scenario. As mentioned previously, see also Figure 19, both the 310S and 800H samples were fabricated from tubing delivered in a bright annealed condition. It should be noted that Alloy 800H exhibited a heteroge-

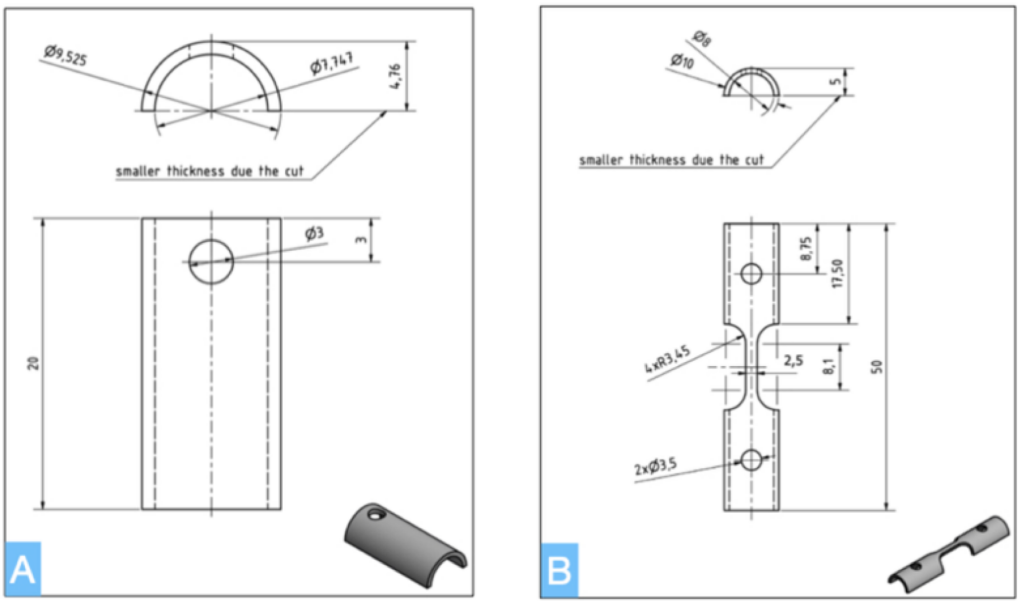

Figure 19: Geometry of the specimens used for the immersion corrosion tests and the SSRT tests. Left (A): immersion specimens for Alloy 800H. Right (B): tensile specimen geometry used for the stress corrosion cracking (SSRT) tests with steel 310S.

neous grain size distribution, with finer grains near the surface and coarser grains at the core. In contrast, AISI 310S displayed a homogeneous grain size distribution. The EBSD analysis in both materials revealed an increased local misorientation near the surface, highlighted by the green color in the misorientation maps in Figure 20. This can be correlated with plastic deformation.

The corrosion response of the studied materials under previously described supercritical water (SCW) conditions was assessed using two types of tests: exposure tests and slow strain rate tests, following the internal procedure published in ECC-SMART Deliverable 2.1 [15]. These experiments were carried out in several laboratories participating in the project, including CNL, RATEN, CVR, STUBA, JRC, CIEMAT, SJTU, and UCT. All autoclaves used were recirculating, except one static autoclave used at RATEN. CIEMAT and CNL performed corrosion tests at 23 MPa. In addition, oxide layers formed on the material surfaces were characterized using various microscopy and surface analysis techniques, including Scanning Electron Microscopy (SEM), Focused Ion Beam (FIB), Energy Dispersive X-ray Spectroscopy (EDX), Auger Electron Spectroscopy (AES), and X-ray Photoelectron Spectroscopy (XPS). A more detailed analysis of oxide layer defects was carried out by STUBA using Positron Annihilation Spectroscopy (PAS) [56]. The following section summarizes the most relevant findings.

Results of Corrosion Tests in SCW

The corrosion test results were evaluated primarly by weight gain and oxide thickness. The maximum weight gain results obtained at 380°C and 500°C from all participants are shown in Figure 21. As can be seen, at both temperatures, the weight gains calculated for steel 310S and Alloy 800H were lower than 20 mg/dm^2; such low weight gains are indicative of high corrosion resistance. It should also be noted that although both materials exhibit excellent behavior, steel 310S shows slightly better performance than Alloy 800H at 500 ºC in terms of weight gain, although the dif-

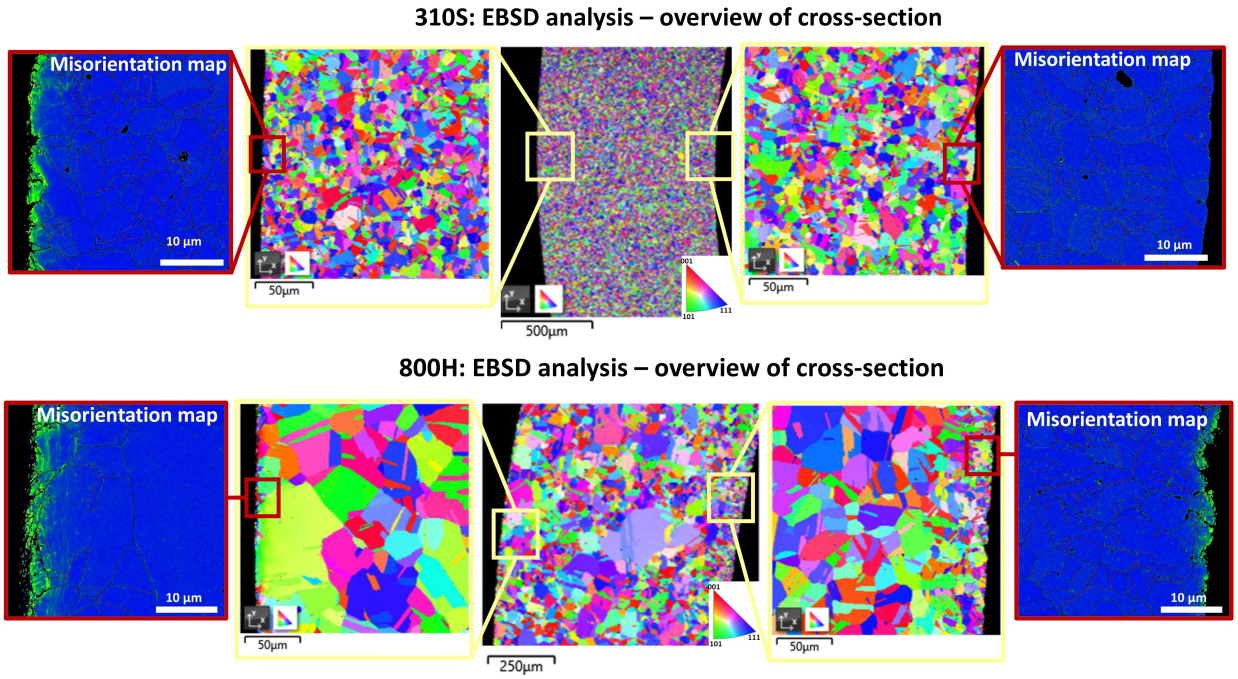

Figure 20: Inverse pole and local misorientation EBSD maps for steel 310S (upper) and Alloy 800H (lower). The highlighted green regions in the misorientation maps indicate zones with higher local misorientation.

ference is not considered significant. A notable feature of the dataset is that the scatter between laboratories is significantly larger at 380°C than at 500°C. This is consistent with the sharp drop in water density, dielectric constant, and ion product across the critical region. These changes can strongly affect corrosion processes, resulting in scattered or inconsistent data. Therefore, while the results at 380°C are included for completeness, they should be interpreted with caution.

The results obtained at 500°C were significantly more homogeneous, with less variability between laboratories. This is attributed to the fact that, at 500°C, the system is in a gas-like thermodynamic state, with reduced fluctuations of material fluid properties properties of water. Unique long-term tests with durations up to 7,000 h were performed by JRC, CNL, RATEN, and SJTU. Part of these data were used to refine the corrosion model for fuel cladding, Novotný and Guzonas [57]. The data were found to follow mainly a logarithmic law fit, and changes in weight gains are minimized after approximately 3,000 hours in the case of exposures at 500°C, as shown by Khumsa-Ang et al. [46]. In contrast, for exposures at 380°C, no comparable steady state was observed. These trends were supported by complementary microstructural and electrochemical investigations. Slow Positron Beam Analysis (SPBA) indicates that at 380°C, both alloys form comparatively porous oxide scales, whereas at 500°C the porosity in both alloys decreased. Auger electron spectroscopy and selected XPS analyses performed by CIEMAT confirm that Cr is incorporated into the oxide layers of both alloys and becomes the dominant oxide-forming element at 500°C. However, a subsequent cross-sectional analysis of both alloys revealed several features that must be taken into account for the selection of materials, such as localized internal oxidation; see Figure 22.

Steel 310S and Alloy 800H show a thin and compact oxide layer, on the order of hundreds of nanometers, locally increased up to 5 µm in thickness; see Figure 22 where specimens were exposed in autoclaves at the Amalia lab in JRC Petten while SEM images were produced in cooperation

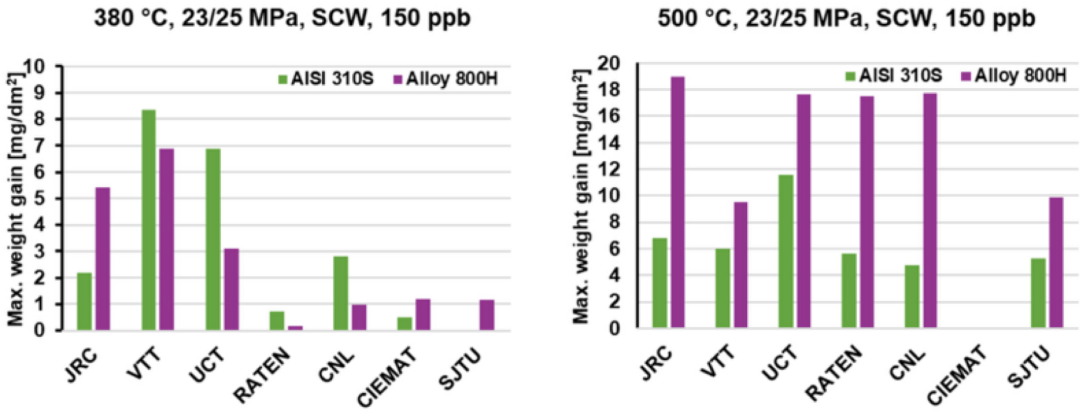

Figure 21: Interlaboratory comparison of maximum weight change values of the AISI 310S and Alloy 800H specimens exposed to SCW at 380°C (left) and 500°C (right).

with CVR. Additionally, SEM/FIB/EDX studies of cross-sections [58] reveal intergranular oxidation, cavities, and Ti-rich inclusions in 800H at both temperatures. In 310S at 380°C, subsurface cracking, internal oxidation, and heterogeneous Cr enrichment were observed in the form of islands; combined with the high strength observed for this material and microstructural evidence, this suggests possible sigma-phase formation in 310S. Despite the favorable performance of these alloys under the selected test conditions, these microstructural features should be taken into account in subsequent stages of material manufacturing and qualification.

Results from corrosion tests were supported and complemented by electrochemical measurements performed in supercritical water (SCW). Electrochemical impedance spectroscopy (EIS) carried out at 150 ppb and higher O_2 levels, confirmed that the overall effect of oxygen content on general corrosion rates is modest, confirming the previously reported results by Macák et al. [59] and Valtr et al. [60]. The electrochemical measurements confirmed local corrosion-rate peaks near the critical region (360–380°C, 22–25 MPa), as previously predicted by Guzonas and Cook [61]. This is related to the prevalence of electrochemical reactions over chemical oxidation, which is pronounced until around 450°C, see Imre et al. [62]. All these results further confirm the sharp changes in the physico-chemical properties of water and therefore explain the scattered results obtained between the partners who performed exposure tests at 380°C. Although temperature is a key factor that increases the kinetics of corrosion processes, the instability of the system near the phase transition, along with the localized corrosion peak rates observed around 380°C, may promote localized degradation phenomena such as pitting corrosion. These effects should be carefully considered in the design of fuel assembly components operating near the pseudo-critical region.

An extrapolation of oxide thickness data obtained in laboratory tests up to 7,000 h was performed to estimate the behavior at 30,000 h, which approximately corresponds to a full fuel cycle. Preliminary results based on a power law fit indicate projected oxide thicknesses below 5 µm for both materials, further supporting their high corrosion resistance even over extended operation times. The penetration of the wall of the cladding after 30,000 h of operation was found to be below 1 µm Novotný and Guzonas [57] for both materials, which is well below the 140 µm limit established in the HPLWR project Schulenberg [63]. Additionally, a preliminary estimation of metal loss (wall penetration) was carried out. The data obtained were used to refine the model developed by Guzonas et al. [64].

Overall, Alloy 800H and steel 310S showed broadly similar corrosion behavior in supercritical

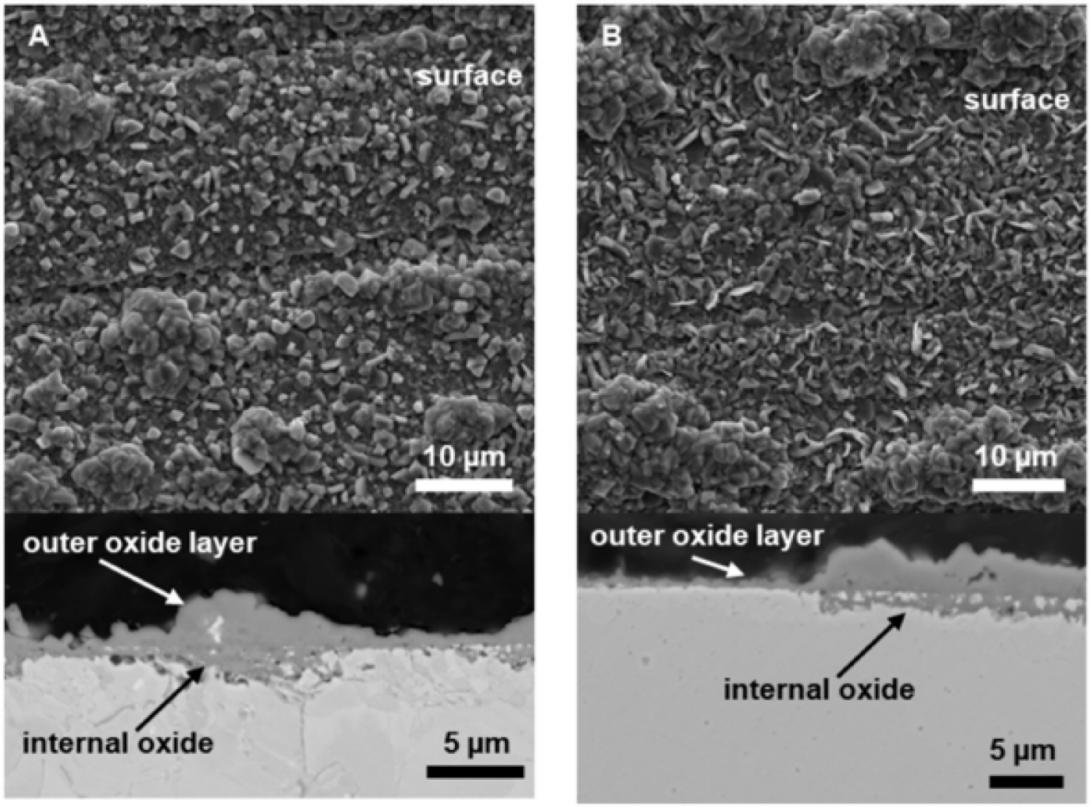

Figure 22: Outer surface and cross-section of specimens exposed at 500°C in SCW, with 150 ppb DO, for 7,000 h. Left A: 310S. Right B: 800H.

water at the selected temperatures. The decisive discriminator comes from separate-effects tests under LOCA-like conditions (approximately 0.1 MPa, 1,200°C, tens of hours) [15; 65]. In these experiments, 310S, 800H, and an AFA alloy all outperformed conventional zirconium-based claddings. Alloy 800H exhibited weight gains on the order of 500 mg/dm^2. In contrast, steel 310S showed a net mass loss exceeding 10,000 mg/dm^2, irrespective of exposure time, as a result of extensive oxide spallation.

The experimental AFA steel exhibited a non-homogenized microstructure, with a mixture of small grains (tens of micrometers) and very large grains (200 µm).

At 380°C, the results show a large scatter: the base material exhibits net weight losses of up to approximately 7,000 h, beyond which the oxide scale can stabilize, while the heat-treated material shows net weight gains over the same exposure period. This behavior can be explained as consistent with the strong variations in physicochemical properties controlling corrosion processes in the vicinity of the thermodynamic critical point of water. At 500°C, both conditions show weight gains, but these are clearly smaller for the heat-treated material, most likely due to the development of a passive layer based on Al_2O_3. However, it is necessary to point out that the heat treatment (HT) performed at 850°C for 50 h in air results in the formation of secondary phases, which may have a detrimental effect on mechanical properties and may promote inner oxidation, as can be seen in Figure 23.

Regarding the study on stress corrosion cracking susceptibility of 800H and steel 310S, an SSRT program was successfully designed, including a loading system for semi-tubular 800H and

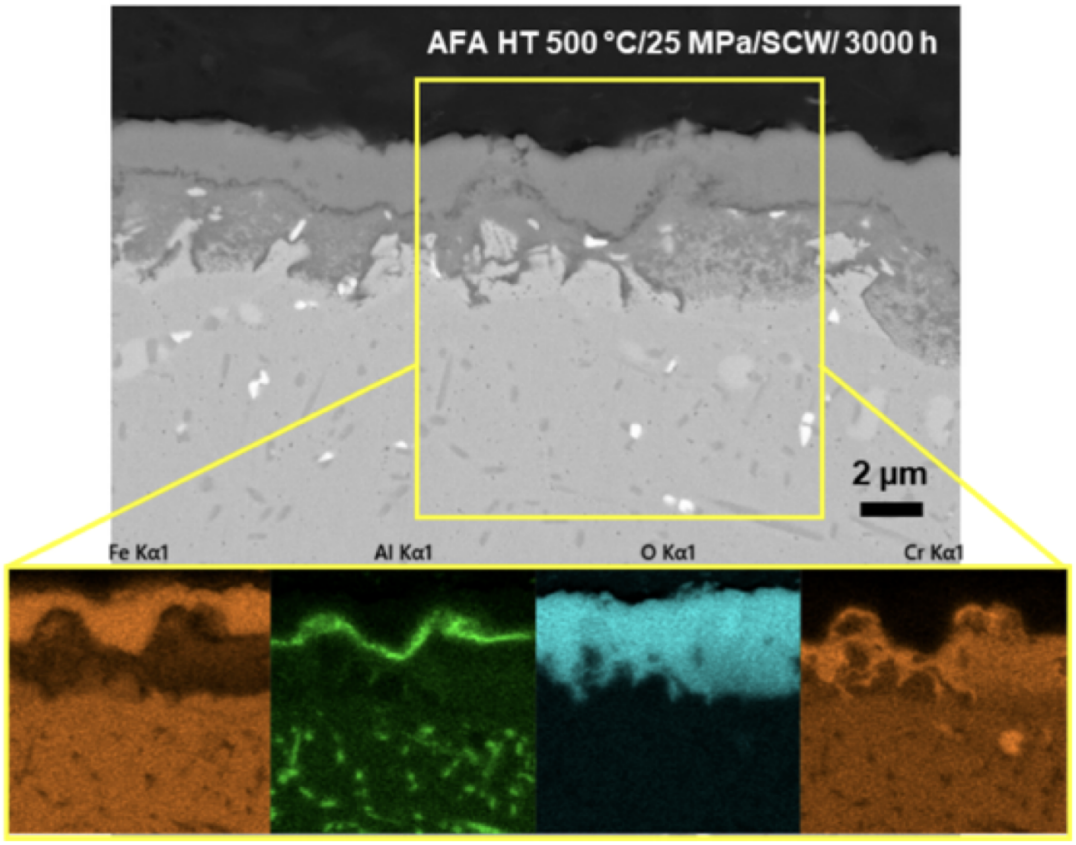

Figure 23: AFA HT after exposure in SCW at 500°C for 3,000 h. The exposure was carried out by JRC in the Amalia lab. The SEM image is accompanied by a detailed EDS map with selected alloying elements (CVR).

310S specimens. The tests were performed in air and supercritical water (SCW) at 380 and 500°C with creep-regime strain rates of 10^{-6} and 10^{-7} s^{-1}. Stainless steel 310S exhibited significantly higher yield and ultimate tensile strengths than 800H under all conditions, whereas 800H sustained higher plastic strains, i.e., showed greater ductility. Under the tested conditions, SSRT tests in SCW did not demonstrate a clear increase in SCC susceptibility: at 380°C (in both air and SCW) no intergranular cracking was detected, and failure was governed by plastic deformation and ductile fracture, with only a few shallow transgranular crack initiations. At 500°C in SCW, shallow intergranular cracks were observed in both alloys, but they remained confined to a few grains from the surface, arrested at the interface with the unaffected bulk, and final failure again occurred by ductile fracture. For steel 310S, similar shallow intergranular (IG) indications in air at 500°C indicate that the combined effect of applied strain rate and a sensitized or highly strained subsurface microstructure is sufficient to initiate such cracks, and that the specific contribution of SCW could not be clearly isolated. In 800H, most IG cracks at 500°C in SCW are consistent with an IGSCC mechanism driven by the synergy of environment, applied stress, and strained subsurface microstructure, although these cracks remained very small and did not dominate the overall failure mode. These results were also compared with data from previous projects that employed different specimen geometries (e.g., cylindrical or flat samples), and no significant influence of specimen geometry on the stress corrosion cracking susceptibility of either alloy was identified within the

experimental scatter.

From a reactor design perspective, the present results support the feasibility of using Fe-based austenitic alloys such as 310S and 800H as fuel cladding materials in supercritical water-cooled modular reactors. The very limited oxide thickness and wall thinning extrapolated to fuel residence times, together with predominantly ductile failure in SSRT tests and structurally robust and protective oxide scales under normal SCW conditions, provide comfortable margins for integrity against uniform corrosion and stress corrosion cracking. The observed sensitivity of oxidation and electrochemical behavior around the critical thermodynamic temperature is very limited and does not pose a limitation for the reactor core. Operating limits incorporate appropriate safety margins, as indicated in Section 3:

- **Normal operation PCT:** < 625°C (margin to creep limit)
- **Design basis accident PCT:** < 850°C (margin to failure)
- **Fuel centerline temperature:** < 2400°C (margin to melting)
- **Assembly box temperature:** < 550°C (oxidation limit)

From a safety standpoint, the generally thin, Cr-rich, adherent oxides formed by both alloys in SCW protect the fuel cladding from embrittlement and the risk of oxide fragmentation and channel blockage, and are therefore consistent with the overall safety goals of SCW-SMR concepts.

Taking all these results into account, both 800H and 310S can be considered suitable candidates for further material qualification as fuel cladding for supercritical water-cooled small modular reactors. At the same time, the fact that 800H is already qualified for nuclear applications, together with its more favorable behavior under simulated LOCA conditions, should be taken into consideration as part of the selection criteria, rather than as a definitive ranking between the two alloys. The neutronic effects of switching from Zr-based to Fe-based cladding are well recognized and were addressed at the core-physics level (e.g., spectrum hardening, reactivity penalties); yet the differences between 310S and 800H in this respect are expected to be modest compared with their common departure from zirconium alloys.

Irradiation Effects on Corrosion

The SCW environment demands high resistance from structural materials, a situation further complicated by the presence of neutron irradiation. Unfortunately, the high pressure of SCW introduces significant safety risks that are not adequately addressed by current legislation governing research reactors and related infrastructure. Consequently, the absence of in-reactor test facilities necessitated sequential testing approaches—irradiation followed by corrosion testing—as employed in the ECC-SMART project, Šípová et al. [66].

Candidate structural materials such as 310S and 800H were neutron-irradiated in the LVR-15 research reactor, Krechlerova et al. [67], achieving a neutron damage level of 0.3 displacements per atom (dpa). The impact of neutron irradiation was evaluated through a combination of microstructural analysis, mechanical testing, and corrosion testing. In-depth microstructural assessments revealed the formation of fine black dots, see also Kočík and Keilová [68], within the microstructures of both irradiated alloys. Despite the low level of neutron damage, the yield strength was significantly increased at the expense of ductility.

The corrosion behavior of the irradiated specimens was tested under conditions simulating those of SCW-SMR operation. Exposure in SCW reveals no significant differences in weight changes between non-irradiated and irradiated specimens. However, a noticeable Cr-depleted zone was identified beneath the surface, which was particularly evident in the irradiated specimens. An example is

shown in Figure 24, where the depleted Cr zone is highlighted by a grey arrow. EBSD analysis further reveals that the Cr-depleted zone beneath the surface partly underwent recrystallization (blue color in Figure 24(A)). More details can be found in Šípová et al. [66]. EBSD data were collected together with information about the composition. Based on these data, it was found that the oxide layer does not diffract well, and thus no good-quality patterns were provided for indexing; only the base material (310S) is imaged by EBSD (Figure 24(A) and (B)). The lack of reliable diffraction patterns of oxides may be attributed to a combination of factors, including their structural characteristics as well as the specimen preparation method. Typically, the recrystallized new grains are free of strain (blue in Figure 24(A)) and possess different crystallographic orientations (IPF map) compared to the adjacent grains (highlighted in Figure 24(B) by a white arrow).

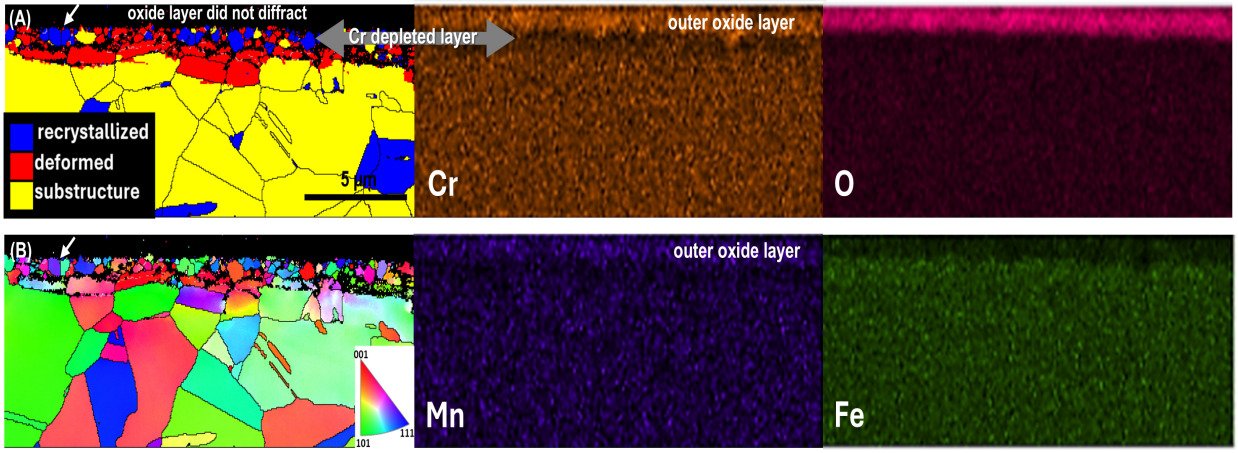

Figure 24: EBSD analysis accompanied by EDS maps of irradiated 310S after exposure to SCW for up to 500 h (CVR data).

In the case of 310S, the chromium content notably reduced to 10 wt.%. This is most likely caused by a higher density of crystal lattice defects induced by neutron irradiation. A more pronounced chromium depletion may lead to the assumption that the resulting oxide layer may offer even greater protective quality. It is a question of how the situation could develop over time and with increasing neutron damage, as it is difficult to predict the synergistic effect of temperature, neutron flux, and radiation damage.

Neutron irradiation remains preferable for mechanical property evaluation due to uniform damage, while proton irradiation allows higher microstructural damage with low activation, simplifying handling. Its shallow penetration is less critical for corrosion, which depends on surface conditions. The proton parameters need refinement to better mimic neutron effects. However, studying these conditions from early exposure is essential for understanding material behavior and advancing next-generation nuclear technologies. Further research should address long-term radiation effects, thermal aging, and microstructural changes under SCW, especially secondary phase formation. Data on irradiated materials remain scarce, underscoring the need for more studies.

6 Proposed Licensing Approach

The state-of-the-art environment for the licensing of nuclear reactors relies to a significant extent on operational experience, and consequently, on proven technologies. The supercritical water-cooled nuclear reactors have not yet participated in commercial operation. The main consequence for the

purpose of this task is therefore lack of operational experience and also technology specific licensing approaches and rules. The main challenges expected in the future licensing of the SCW SMR are illustrated in some detail below, followed by a proposal of a possible licensing approach.

Regulatory Challenges

An extensive review of available documentation has been performed, including the relevant documentation by IAEA, Generation IV International forum (GIF), Western European Nuclear regulators Association (WENRA) and country regulations in Canada, China, Czech Republic, Finland, and United Kingdom, Cizelj et al. [69]. During the review, it was assumed that the ECC-SMART family of designs is actually a combination of three large nuclear power plant families of designs: new (3rd generation) reactors, small modular reactors and 4th generation reactors including the Supercritical Water-Cooled Reactor (SCWR). Such a combination is the conjunction of the three sets of safety elements as long as compatible with ECC-SMART, Figure 25

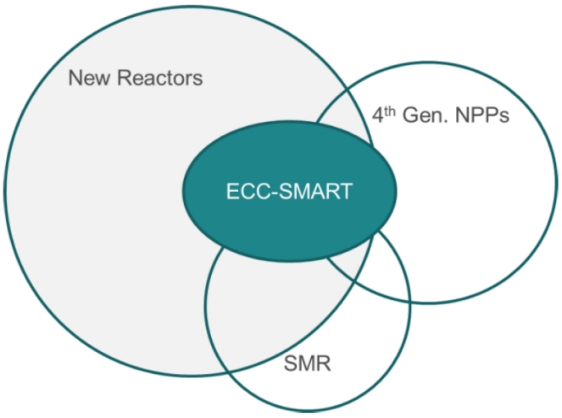

Figure 25: Safety Elements Applicable to the ECC-SMART.

No existing regulatory framework for supercritical water reactors or relevant technology specific licensing or safety rules have been found. Nevertheless, all high-level safety requirements of the IAEA (SSR-2/1) and the GIF have been found to also apply to the ECC-SMART. Some similarities with the boiling water reactors have been noted. The following, non-exhaustive, list of potentially unique licensing challenges for the SCW-SMR have been identified:

- Horizontal fuel assemblies. There is very limited design and operational experience.
- Operating conditions far beyond the pressures and temperatures of current light water reactors (e.g., 500 °C, 25 bar) require implementation and qualification of novel materials.
- Extensive reliance on passive safety is expected, including practical prevention of severe accidents with core melt. This will also require extensive verification and validation.

Proposed Licensing Approach

A graded approach leveraging existing LWR regulations is proposed in the frame of ECC-SMART Duspiva et al. [70]; Prošek and Cizelj [71]:

- Identify the phase of the design development, e.g., pre-conceptual design, conceptual design, basic design, detailed design. The design phase implies the scope of the safety demonstration that has to be developed. This results in an (updated) design description focusing on the data required for safety analysis
- Translate the (updated) legislative requirements into the safety requirements of the design under development.
- Translate the (updated) legislative requirements and safety requirements into the appropriate safety criteria.
- Investigate the state of the art and define the potential need for further experimental support and analytical tool development and validation.
- Design and execute appropriate supporting experimental programs to produce new knowledge or demonstrate the viability of tested systems or equipment, or to qualify individual components or systems.
- Design and execute analytical program(s) to demonstrate fulfilled safety requirements through fulfillment of defined safety criteria

International collaboration on the design and execution of the experimental (e.g., materials for fuel cladding and reactor coolant pressure boundary, horizontal fuel assemblies) and analytical (e.g., heat transfer at operating and accidental conditions) programs needed, including verification and validation, may greatly facilitate the exchange of knowledge and experience between the design groups in Canada, China and Europe. Another important vehicle for faster development and licensing may also be the use of "phased licensing", e.g., increasing licensing requirements with increasing power– and consequently also source term- levels.

7 Economic Considerations and Future Development Path

The economic viability of Small Modular Reactors is among the primary considerations for their future development and deployment. The key economic factors are outlined and briefly discussed below and compared with the expected performance of comparable SMR concepts. This is then followed by a brief description of the near-term development priorities and the vision of the future ECC-SMART family of designs.

Cost Drivers and Potential for Optimization

The EU-SCW-SMR design provides many opportunities to improve the economics as compared to other light water reactor designs. A non-exhaustive list of them follows:

- **High thermal efficiency (44%):** Reduces fuel consumption by 25% versus current LWRs with thermal efficiency below 33%.
- **Simplified balance of plant:** Direct cycle eliminates steam generators both as a very complex structure and as the origin of non-negligible heat losses.
- **Compact design:** Smaller containment and auxiliary buildings as compared with the pressurized water reactors, which dominate the commercial reactor fleet today.

- **Factory fabrication potential:** The modular construction approach of reactors of comparatively smaller power facilitates fabrication and construction of major safety-related components in the factory. Immediate benefits include production in controlled conditions (quality assurance) and transportability of the equipment to the sites away from the major water ways, e.g., to the remote communities.
- **Extended fuel cycle:** Target 18-24 month refueling interval may be comparable to or longer than refueling intervals of the competitive light water designs with relatively low power and therefore also considerable leakage of neutrons.

Table 9 compares the SCW-SMR with other SMR technologies under development. Brief com-

Table 9: Comparison of SCW-SMR with competing SMR technologies based on the publicly available documents

Parameter	**SCW-SMR**	**iPWR**	**BWR-SMR**	**HTGR**	**MSR**
Power (MWe)	128	50-300	50-300	50-200	100-300
Efficiency (%)	44	33	34	42	45
Outlet temp. (°C)	500	320	285	750	700
Technology readiness	Medium	High	High	Medium	Low
Passive safety	Excellent	Good	Good	Excellent	Good

parison of main features of the SCW-SMR and some other selected SMR designs is given in Table 9. It may also be noted that the EU-SCW-SMR design, to a significant extent, builds on the design and operational experience of (boiling) light-water cooled reactors and conventional supercritical water-cooled thermal power plants.

Deployment Scenarios

The EU-SCW-SMR design with 290 MWth (∼130 MWe) power level suits multiple applications beyond the current deployment of the light water-cooled reactors. A non-exhaustive list of possible applications includes:

- Supply electricity and heat to remote communities.
- Supply quality heat (outlet up to 500°C) to industrial processes, including hxdrogen generation, with optional cogeneration of electricity.
- Provide back-up for renewables and/or stabilize renewable-dominated grids.
- Replace retired fossil power plants.

The potential economic advantages, including a wide variety of possible deployment scenarios, support further development of the EU-SCW-SMR design, as briefly outlined below.

Near-Term Priorities

The rather obvious near-term research priorities aiming to optimize the design and verify its safety include:

- Experimental validation of horizontal assembly thermal-hydraulics;

- Integral test facility for natural circulation confirmation;
- Materials irradiation testing under SCW conditions,
- Detailed 3D neutronic calculations with burnup;
- Control rod mechanism development and testing.

Vision

ECC-SMART and previous international and national projects have deepened knowledge of supercritical water. Many well-experienced engineers have thus been trained and become fascinated by nuclear technology. However, all the benefits and perspectives that SCW may possess are described in numerous papers and books. To support further development, natural circulation should be verified in the horizontal core configuration. A full-scale component testing device should be designed and constructed. Such a facility should enable thermal-hydraulic experiments and long-term exposure under simulated operation conditions, including chemistry management. Parallel efforts should focus on extended accident scenario analyses and early engagement with regulators to define SCW-specific licensing requirements. Safety of the concept SCW-SMR should be demonstrated by a prototype of control rod mechanisms, along with optimising burnable absorber strategies for two-year fuel cycles. Supporting activities include developing a training simulator concept and preparing a business case with stakeholder engagement to secure industrial and financial commitment for the construction of the first-of-a-kind demonstration reactor (10-30 MWth).

8 Conclusions

This paper has presented the design concept and comprehensive analysis of the European Supercritical Water-Cooled SMR developed within the ECC-SMART project. The 290 MW_{th} reactor operating at 25 MPa with core outlet temperatures of 500 °C represents a significant advancement in Generation IV reactor technology, achieving thermal efficiencies approaching 44% while demonstrating enhanced passive safety capabilities suitable for near-term deployment.

Principal Findings

The innovative horizontal fuel assembly configuration with seven sequential heat-up stages successfully addresses fundamental challenges identified in previous SCWR concepts. The key technical achievements demonstrated through this work include:

Thermal-hydraulic performance. Subchannel analyses confirm that peak cladding temperatures remain below 625 °C during normal operation, with hot channel factors of 1.15 for enthalpy rise. The seven-stage configuration with intermediate mixing zones effectively reduces thermal peaking and maintains acceptable temperature distributions across all core regions.

Passive safety demonstration. Comprehensive safety analyses using dual independent system codes (RELAP5 and APROS) demonstrate that the design can manage design basis accidents, including Long-Term Station Blackout and Large-Break Loss-of-Coolant Accidents (LBLOCA), without operator intervention or AC power for periods exceeding 72 hours. Peak cladding temperatures during the most challenging LBLOCA scenario reach 780 °C, remaining well below the 850 °C design limit. The horizontal core configuration enables robust multi-loop natural circulation patterns that provide redundant heat removal paths, with primary circulation through isolation

condensers, inter-stage circulation through mixing channels, and intra-assembly circulation due to density stratification.

Materials qualification. Extensive corrosion testing of candidate fuel cladding materials (310S stainless steel and Alloy 800H) at temperatures up to 500 °C and exposure times up to 7,000 hours demonstrates excellent corrosion resistance. Weight gains remained below 20 mg/dm^2 for both materials, and extrapolated wall penetration after 30,000 hours of operation is projected to be below 1 µm, well within the 140 µm limit established in previous HPLWR studies. Slow strain rate tests confirm predominantly ductile failure modes with no significant stress corrosion cracking susceptibility under simulated operating conditions.

Neutronics and core physics. Monte Carlo neutronic analyses using Serpent 2 confirm strongly negative reactivity coefficients: coolant temperature coefficient of -16.8 ± 1.6 pcm/K, moderator temperature coefficient of -10.6 ± 0.5 pcm/K, and fuel temperature coefficient of -1.3 ± 0.2 pcm/K. These coefficients provide inherent stability and substantial safety margins. The core design demonstrates feasibility of a two-year burnup cycle without fuel shuffling, with adequate shutdown margin maintained throughout the cycle even with the most reactive control rod stuck out.

Design Innovations

The European SCW-SMR introduces several innovations that distinguish it from previous SCWR concepts:

The horizontal core configuration eliminates siphon effects that prevented natural circulation in earlier three-pass vertical designs, enabling passive residual heat removal through buoyancy-driven flow. The seven-pass flow scheme with intermediate mixing zones reduces peak cladding temperatures by equalizing coolant enthalpy distribution between stages. Wire-wrapped fuel rod spacers enhance in-assembly mixing while reducing pressure drop compared to grid spacers. The strategic use of subcooled water inventory at 280 °C as a thermal buffer eliminates requirements for high-pressure emergency injection systems, and transverse control rod insertion simplifies drive mechanisms while improving accessibility for maintenance.

Validation and Confidence

The use of multiple independent computational tools throughout this work—RELAP5 and APROS for system thermal-hydraulics, ASSERT-PV SC and STAFAS for subchannel analysis, Serpent 2, MCNP 6.2, and OpenMC for neutronics—provides robust cross-validation of results. Agreement between independent predictions, typically within 10–15% for key safety parameters, validates the fundamental understanding of system behavior and increases confidence in the design's viability. The coupled neutronic-thermal-hydraulic analyses capture essential feedback mechanisms between power distribution and coolant density changes, confirming that negative reactivity feedback provides substantial inherent safety margins during transients.

Remaining Challenges and Future Work

Several areas require continued development before the concept can advance to detailed design and licensing:

Experimental validation of heat transfer correlations for supercritical water under low-flow and horizontal flow stratification conditions remains a priority. Construction of an integral test facility is essential for confirming natural circulation performance in the seven-stage horizontal configuration. Long-term irradiation testing of candidate cladding materials under prototypic neutron

fluences and SCW conditions is necessary to qualify 310S and/or 800H for fuel service. Development of SCW-specific regulatory frameworks through early engagement with licensing authorities will be critical for establishing acceptable safety criteria and demonstration requirements. Finally, detailed engineering of fuel assembly support structures, control rod mechanisms, and manufacturing processes for sandwich-construction assembly boxes requires resolution before proceeding to conceptual design.

Broader Significance

The European SCW-SMR concept offers a promising pathway toward sustainable, economical, and inherently safe nuclear power generation. By combining the only Generation IV light water reactor concept with small modular deployment, the design leverages extensive operational experience from conventional LWRs and mature supercritical technology from fossil power plants while achieving the enhanced safety and efficiency goals of advanced reactor programs. The thermal efficiency approaching 44% reduces fuel consumption by approximately 25% compared to current LWRs, while the direct cycle and compact design offer potential for significant capital cost reductions.

The successful completion of the ECC-SMART project, involving collaboration among European, Canadian, and Chinese research institutions, demonstrates the value of international cooperation in advancing complex nuclear technologies. The comprehensive technical basis established through this work: spanning thermal-hydraulics, safety analysis, materials science, neutronics, and regulatory assessment; provides a solid foundation for progression toward demonstration reactor construction and eventual commercial deployment, contributing to global decarbonization goals while addressing energy security concerns.

Acknowledgments

This work was supported by the European Commission under the ECC-SMART project (Grant Agreement ID: 945234, Horizon 2020 Framework Programme). The authors acknowledge the invaluable contributions from all consortium partners: Budapest University of Technology and Economics, Centro de Investigaciones Energéticas, Medioambientales y Tecnológicas, Research Centre Řež, European Nuclear Education Network, IPP Center, Joint Research Centre Petten, Jožef Stefan Institute, Karlsruhe Institute of Technology, Kungliga Tekniska Hoegskolan, Regia Autonome Tehnologii Pentru Energia Nucleara, Slovenska Technicka Univerzita v Bratislavě, University of Nottingham, University of Sheffield, University of Pisa, Vysoká Škola Chemicko-Technologická v Praze, Valtion teknillinen tutkimuskeskus, (Europe); Canadian Nuclear Laboratories, Carlton University (Canada); Nuclear Power Institute of China, Shanghai Jiaotong University, Xi'an Jiaotong University (China). Part of the results presented were obtained using the CICRR infrastructure, which was financially supported by the Ministry of Education, Youth and Sports of the Czech Republik - project LM2023041. The authors thank the International Atomic Energy Agency and Generation IV International Forum for providing forums for technical exchange and peer review.

References

[1] GIF. Technology roadmap update for generation IV nuclear energy systems. Technical report, OECD Nuclear Energy Agency, Paris, 2014.

[2] I. L. Pioro, editor. *Handbook of Generation IV Nuclear Reactors.* Elsevier Ltd., 1 edition, 2016.

[3] D. T. Ingersoll and M. D. Carelli, editors. *Handbook of Small Modular Nuclear Reactors*. Elsevier Ltd., 2 edition, 2021.

[4] ECC-SMART Consortium, EU Grant Agreement ID: 945234. Project webpage. `https://cordis.europa.eu/project/id/945234`, 2020. last visited: 02.01.2026.

[5] T. Schulenberg and I. Otic. Concept of a small modular SCWR with horizontal fuel assemblies. *ASME Journal of Nuclear Engineering and Radiation Science*, 8(3):031104, 2022. URL `https://doi.org/10.1115/1.4052191`.

[6] European SMR pre-Partnership. Market potential of SMRs in europe. Technical report, European Commission, Brussels, 2023. URL `https://single-market-economy.ec.europa.eu/industry/industrial-alliances/european-industrial-alliance-small-modular-reactors_en`. also available at `https://snetp.eu/wp-content/uploads/2023/07/European-SMR-pre-Partnership-WS1_MarketAnalysis_FinalReport-3July2023.pdf`.

[7] T. Schulenberg and J. Starflinger. *High Performance Light Water Reactor—Design and Analysis*. KIT Scientific Publishing, Karlsruhe, Germany, 2012. ISBN 978-3-86644-817-9.

[8] Y. Oka, S. Koshizuka, Y. Ishiwatari, and A. Yamaji. *Super Light Water Reactors and Super Fast Reactors: Supercritical-Pressure Light Water Cooled Reactors*. Springer, Boston, 2010.

[9] I. Pioro. *Handbook of Generation IV Nuclear Reactors*. Woodhead Publishing, Cambridge, 2 edition, 2023.

[10] Akifumi Yamaji, Koki Matsuoka, Kota Sumida, and Kohki Funatsu. Scope of conceptual development of resilient supercritical light water-cooled reactor (scwr-r). *Nuclear Engineering and Design*, 416:112756, 2024. ISSN 0029-5493. doi: https://doi.org/10.1016/j.nucengdes.2023.112756. URL `https://www.sciencedirect.com/science/article/pii/S0029549323006052`.

[11] M. Yetisir et al. Development and integration of canadian SCWR concept with counter-flow fuel assembly. *Journal of Nuclear Engineering and Radiation Science*, 1(1):011006, 2013.

[12] A. Nava-Dominguez, X. Huang, M. Gaudet, K. Khumsa-Ang, A. D. Mendoza España, J. Chow, D. Roubtsov, and H. K. Namburi. Progress on a Preconceptual Supercritical Water-Cooled Small Modular Reactor. *ASME Journal of Nuclear Engineering and Radiation Science*, 11 (3):031301, jul 2025. doi: 10.1115/1.4068326. URL `https://doi.org/10.1115/1.4068326`. Paper No: NERS-24-1133.

[13] International Atomic Energy Agency. Status of research and technology development for supercritical water cooled reactors. Technical Report 1869, International Atomic Energy Agency, Vienna, Austria, 2019. URL `www.iaea.org`.

[14] A. Nava-Dominguez et al. Report on pre-conceptual design requirements for ecc scw-smr. Technical Report Deliverable D3.6, ECC-SMART, 2025.

[15] A. Sáez-Maderuelo et al. Test matrix based on available materials. Technical Report Deliverable 2.1, ECC-SMART, EU Grant Agreement Number: 945234, 2020.

[16] ECC-SMART Consortium, EU Grant Agreement ID: 945234. Deliverables D2.1, D2.2, D3.2, D3.3, D3.4, D3.6, D4.2, D4.3, D5.1, D5.3, D5.4. European Commission CORDIS Database, `https://cordis.europa.eu/project/id/945234/reporting`, 2024.

[17] T. Schulenberg and I. Otic. Suggestion for design of a small modular SCWR. In *Proc. 10th International Symposium on SCWRs (ISSCWR-10)*, number Paper ISSCWR10-019, Prague, March 15–19 2021.

[18] T. Schulenberg and I. Otic. Conceptual design of structures around the reactor core. Technical Report Project document, ECC-SMART, 2021.

[19] Armando Nava-Dominguez, Xianmin Huang, and Songyu Liu. Studies of the thermalhydraulics subchannel code assert-pv 3.2-sc for supercritical applications. *Journal of Nuclear Engineering and Radiation Science*, 11(2):021402, 11 2024. ISSN 2332-8983. doi: 10.1115/1.4066523. URL `https://doi.org/10.1115/1.4066523`.

[20] W. Ambrosini, I. Otic, T. Schulenberg, A. Pucciarelli, O. Chaaraoui, T. Varju, A. Kiss, B. Babcsány, Cs. Antók, P. Mészáros, Z. Bertesina, Sz. Czifrus, V. Filonov, D. Fedorov, Y. Filonova, Y. Dubyk, A. Nava-Dominguez, and X. Zhao. Report on the preconceptual studies on the core layout and passive safety concept of the SCW-SMR. Technical Report Deliverable D3.3, ECC-SMART, 2024.

[21] T. Varju, A. Kiss, Cs. Antók, B. Babcsány, I. Boros, P. Mészáros, Z. Bertesina, and Sz. Czifrus. Current results of BME NTI in the ECC-SMART project: Different analysis on the SCW-SMR. In *Proc. ICONE31 Conference*, Prague, Czech Republic, August 4–8 2024. doi: 10.1115/ICONE31-135760. URL `https://doi.org/10.1115/ICONE31-135760`.

[22] RELAP5. Webpage. `https://inl.gov/relap53d/`. last visited: 17.11.2025.

[23] APROS. Webpage. `https://www.apros.fi/`. last visited: 16.11.2025.

[24] O. Chaaraoui, A. Pucciarelli, W. Ambrosini, I. Otic, T. Schulenberg, C. Allison, and Z. Fu. Customising a system code for the analysis of the thermal-hydraulic behavior of a supercritical pressure light water small modular reactor. In *Proc. 31st Int. Conf. on Nuclear Engineering (ICONE31)*, Prague, Czech Republic, August 4–8 2024.

[25] X. Zhao et al. Report on the improved system codes describing how they improved. Technical Report Deliverable D3.4, ECC-SMART, 2025.

[26] Jaakko Leppänen, Maria Pusa, Tuomas Viitanen, Ville Valtavirta, and Toni Kaltiaisenaho. SERPENT a continuous-energy monte carlo reactor physics burnup calculation code: User's manual. `https://serpent.vtt.fi/`, 2015. Version 2.1.23.

[27] I. Otic et al. Report summarizing the newly generated reference data for natural convection, forced and mixed convection and decay heat removal. Technical Report Deliverable D3.1, ECC-SMART, 2024.

[28] S. Kassem, A Pucciarelli, and W. Ambrossini. Analysis of existing correlations for heat transfer to supercritical pressure fluids in support to the ecc-smart project. Technical report, ECC-SMART, 2021.

[29] X. Zhao et al. Report on the results of the benchmark exercise. Technical Report Deliverable D3.2, ECC-SMART, 2023.

[30] S. Kassem et al. Heat transfer enhancement in supercritical fluids considering surface roughness effects. *International Journal of Heat and Mass Transfer*, 202:123654, 2023.

[31] W. Ambrosini et al. Report on the pre-conceptual studies on the core layout and passive safety concept of the SCW-SMR. Technical Report Deliverable D3.3, ECC-SMART, 2025.

[32] T. Varju, Cs. Antók, P. Mészáros, and B. Babcsány. Coupled reactor physics and thermal hydraulics analysis of an SCW-SMR reactor concept – part II: Improvement of the concept and sensitivity analyses. *Annals of Nuclear Energy*, 217:111221, 2025. doi: 10.1016/j.anucene.2025.111221.

[33] Tamás Varju, Boglárka Babcsány, Péter Mészáros, Csenge Antók, and Szabolcs Czifrus. Coupled reactor physics and thermal-hydraulics analysis of an scw-smr reactor concept – part i: Model development and demonstration. *Annals of Nuclear Energy*, 217:111222, 2025. ISSN 0306-4549. doi: https://doi.org/10.1016/j.anucene.2025.111222. URL https://www.sciencedirect.com/science/article/pii/S0306454925000398.

[34] T. Varju, A. Csige, A. Kiss, V. Filonov, Y. Filonova, D. Fedorov, A. Pucciarelli, S. Kassem, and W. Ambrosini. Discussion and perspectives for improvements of heat transfer correlation capabilities for fluids at supercritical pressures. *Nuclear Engineering and Design*, 421:113085, 2024. doi: 10.1016/j.nucengdes.2024.113085. URL https://doi.org/10.1016/j.nucengdes.2024.113085.

[35] S. Kassem, A. Pucciarelli, and W. Ambrosini. Cfd prediction of heat transfer at supercritical pressure with rough walls: Parametric analyses and comparison with experimental data. *Annals of Nuclear Energy*, 188:109815, 2023. ISSN 0306-4549. doi: https://doi.org/10.1016/j.anucene.2023.109815. URL https://www.sciencedirect.com/science/article/pii/S0306454923001342.

[36] A. Pucciarelli, S. Kassem, and W. Ambrosini. Characterisation of observed heat transfer deterioration modes at supercritical pressure with the aid of a cfd model. *Annals of Nuclear Energy*, 178:109376, 2022. ISSN 0306-4549. doi: https://doi.org/10.1016/j.anucene.2022.109376. URL https://www.sciencedirect.com/science/article/pii/S0306454922004108.

[37] Attila Kiss and Balázs Kiss. Discussing cfd analysis of horizontal and vertical upward flow under supercritical conditions. In *Proceedings of the 11th International Symposium on Supercritical Water-Cooled Reactors*, pages 829–841. Pisa University Press, 2025. ISBN 979-12-5608-133-2.

[38] Kenneth Chinembiri, Shuisheng He, and Wei Wang. A study of the effect of pyramid roughness on turbulent heat transfer in supercritical water. In *Proceedings of the 11th International Symposium on Supercritical Water-Cooled Reactors*, pages 783–793. Pisa University Press, 2025. ISBN 979-12-5608-133-2.

[39] J. Leppänen et al. The Serpent monte carlo code: Status, development and applications in 2013. *Annals of Nuclear Energy*, 82:142–150, 2015. doi: 10.1016/j.anucene.2014.08.024. URL https://doi.org/10.1016/j.anucene.2014.08.024.

[40] C. J. Werner, J. C. Armstrong, F. B. Brown, J. S. Bull, L. Casswell, L. J. Cox, D. A. Dixon, R. A. Forster III, J. T. Goorley, H. G. Hughes III, J. A. Favorite, R. L. Martz, S. G. Mashnik, M. E. Rising, C. J. Solomon Jr., A. Sood, J. E. Sweezy, A. J. Zukaitis, et al. MCNP User's

Manual, Code Version 6.2. Technical Report LA-UR-17-29981, Los Alamos National Laboratory, Los Alamos, NM, USA, October 2017. URL https://mcnp.lanl.gov/pdf_files/TechReport_2017_LANL_LA-UR-17-29981_WernerArmstrongEtAl.pdf.

[41] Paul K. Romano, Nicholas E. Horelik, Bryan R. Herman, Adam G. Nelson, Benoit Forget, and Kord Smith. OpenMC: A State-of-the-Art Monte Carlo Code for Research and Development. *Annals of Nuclear Energy*, 82:90–97, August 2015. doi: 10.1016/j.anucene.2014.07.048. URL https://doi.org/10.1016/j.anucene.2014.07.048.

[42] Boglárka Babcsány, Valerio Giusti, Andreea Moise, Péter Mészáros, Szabolcs Czifrus, and Jimmy C Chow. Results and lessons learned from the generation iv scwr-fqt comprehensive monte carlo computational benchmark. *Annals of Nuclear Energy*, 191, 2023. ISSN 0306-4549. doi: 10.1016/j.anucene.2023.109903. URL https://doi.org/10.1016/j.anucene.2023.109903.

[43] Cs. Antók, Sz. Czifrus, and V. Giusti. Neutronic calculations for preliminary core design of SCW-SMR. *Annals of Nuclear Energy*, 209:110805, 2024. doi: 10.1016/j.anucene.2024.110805. URL https://doi.org/10.1016/j.anucene.2024.110805.

[44] Valerio Giusti. Two-dimensional fuel assembly study for a supercritical water-cooled small modular reactor. *J. Nucl. Eng.*, 6(3)(26), 2025. doi: 10.3390/jne6030026. URL https://doi.org/10.3390/jne6030026.

[45] B. Cox. Accelerated oxidation of zircaloy-2 in supercritical steam. Technical Report AECL-4448, Atomic Energy of Canada Limited, 1973.

[46] Kittima Khumsa-Ang et al. A state-of-the-art review of the supercritical water-cooled reactor technology: part ii materials and chemistry. *Nuclear Engineering and Design*, 446, 2026.

[47] W. Cook, J. Miles, and R. Hui. Zirconium oxide coatings on p91 and zircaloy substrates for use in scwrs. In *32nd Annual Conference of the Canadian Nuclear Society and 35th CNS/CNA Student Conference*, Sheraton on the Falls, Niagara Falls, Ontario, Jun 5–8 2011.

[48] T. R. Allen, Y. Chen, X. Ren, K. Sridharan, L. Tan, G. S. Was, E. West, and D. A. Guzonas. Material performance in supercritical water. In R. J. M. Konings, editor, *Comprehensive Nuclear Materials*, volume 5, pages 279–326. Elsevier, 2011.

[49] M. Payet, L. Marchetti, M. Tabarant, and J. P. Chevalier. Corrosion mechanism of a ni-based alloy in supercritical water: Impact of surface plastic deformation. *Corrosion Science*, 100: 47–56, 2015. doi: 10.1016/j.corsci.2015.06.032.

[50] Nuclear Energy Agency (NEA). Committee on the Safety of Nuclear Installations. Irradiation embrittlement and optimisation of annealing. 1993. URL https://inis.iaea.org/records/332ey-yx426.

[51] Y. Behnamian, Amir Mostafaei, Alireza Kohandehghan, Beniamin Zahiri, Wenyue Zheng, David Guzonas, Markus Chmielus, Weixing Chen, and Jing Li Luo. Corrosion behavior of alloy 316l stainless steel after exposure to supercritical water at 500°c for 20,000h. *The Journal of Supercritical Fluids*, 127:191–199, 2017. doi: 10.1016/j.supflu.2017.03.022.

[52] M. Edwards, S. Rousseau, R. Novotný, B. Gong, M. Fulger, S. Penttilä, A. Toivonen, A. Sàez-Maderuelo, L. Zhang, D. Guzonas, and X. Huang. The reproducibility of corrosion testing

in supercritical water—results of a second international interlaboratory comparison exercise. *Journal of Nuclear Materials*, 565:153759, 2022. doi: 10.1016/j.jnucmat.2022.153759.

[53] Y. Liu, L. Gou, X. Leu, et al. The mechanism of abnormal corrosive behavior of metallic materials in the pseudocritical region of supercritical water. *Materials Today Communications*, 35:105817, 2023. doi: 10.1016/j.mtcomm.2023.105817.

[54] T. M. Hayward, I. M. Svishchev, and R. C. Makhija. Stainless steel flow reactor for supercritical water oxidation: corrosion tests. *The Journal of Supercritical Fluids*, 27:275–281, 2003. doi: 10.1016/S0896-8446(02)00264-4.

[55] NRC Regulations. Title 10, code of federal regulations, § 50.46 acceptance criteria for emergency core cooling systems for light-water nuclear power reactors. Technical report, 2024. URL `https://www.nrc.gov/reading-rm/doc-collections/cfr/part050/part050-0046.html`.

[56] J. Degmová, Y. Song, B. Li, S. Sojak, X. Cao, R. Novotný, M. Novák, W. Egger, and V. Kršjak. A slow positron beam study of the oxidation behaviour of 310s stainless steel and alloy 800ht exposed to supercritical water. *The Journal of Supercritical Fluids*, 202: 106057, 2023. ISSN 0896-8446. doi: https://doi.org/10.1016/j.supflu.2023.106057. URL `https://www.sciencedirect.com/science/article/pii/S0896844623002218`.

[57] R. Novotný and D. Guzonas. Modelling the long-term corrosion behaviour of candidate fuel cladding alloys for a supercritical water-cooled reactor. *Nuclear Engineering and Design*, 446, 2026. doi: 10.1016/j.nucengdes.2025.114571.

[58] R. Novotný et al. Report summarising the results of the out-of-pile corrosion tests. Technical Report Deliverable 2.3, ECC-SMART, 2025.

[59] J. Macák, R. Novotný, P. Sajdl, J. Bystrianský, L. Tůma, and M. Novák. In-situ electrochemical impedance measurements of corroding stainless steel in high subcritical and supercritical water. *Corrosion Science*, 150:9–16, 2019. doi: 10.1016/j.corsci.2019.01.018.

[60] J. Valtr, P. Roztočil, D. Dašek, R. Mušálek, F. Lukáč, J. Klečka, M. Janata, M. Arnoult-Růžičková, E. Mištová, L. Jelínek, P. Sajdl, and J. Macák. Measurement system for in-situ estimation of instantaneous corrosion rate in supercritical water. *The Journal of Supercritical Fluids*, 204:106091, 2024. doi: 10.1016/j.supflu.2023.106091.

[61] D.A. Guzonas and W.G. Cook. Cycle chemistry and its effect on materials in a supercritical water-cooled reactor: A synthesis of current understanding. *Corrosion Science*, 65:48–66, 2012. doi: doi.org/10.1016/j.corsci.2012.08.006. URL `https://doi.org/10.1016/j.corsci.2012.08.006`.

[62] A. R. Imre, U. K. Deiters, T. Kraska, et al. The pseudocritical regions for supercritical water. *Nuclear Engineering and Design*, 252:179–183, 2012. doi: 10.1016/j.nucengdes.2012.07.019.

[63] T. Schulenberg. Material requirements of the high performance light water reactor. *The Journal of Supercritical Fluids*, 77:127–133, 2013. doi: 10.1016/j.supflu.2013.02.008.

[64] D. Guzonas, M. Edwards, and W. Zheng. Assessment of candidate fuel cladding alloys for the canadian supercritical water-cooled reactor concept. *Journal of Nuclear Engineering and Radiation Science*, 2(1):011016, 2016. doi: 10.1115/1.4031502.

[65] M. Šípová et al. Report summarising basic characterization of materials and specimens machining. Technical Report Deliverable 2.2, ECC-SMART, 2021.

[66] M. Šípová, D. Marušáková, J. Vít, J. Křivská, and P. Zháňal. Study of neutron irradiation effects on mechanical properties and corrosion behaviour of 310s and 800h alloys for scw-smr application. *Nuclear Engineering and Design*, 446, Part B:114569, 2026. URL `https://doi.org/10.1016/j.nucengdes.2025.114569`.

[67] A. Krechlerova, M. Košťál, J. Milčák, and J. Kučera. Availability of neutron activation facilities to foreign users at research centre Řež, czech republic. *Journal of Radioanalytical and Nuclear Chemistry*, 333:3559–3564, 2024. URL `https://link.springer.com/article/10.1007/s10967-023-09276-7`.

[68] J. Kočík and E. Keilová. Radiation damage structure in irradiated and annealed 440 wwer reactor pressure vessel steels. 1993.

[69] L. Cizelj, A. Prošek, M. Uršič, J.-C. de la Rosa Blul, O. Martin, A. Kiss, I. Boros, M. Hrehor, A. Toivonen, A. Nava-Dominguez, S. He, and I. Otic. D5.1 safety criteria and requirements for the scw-smr concept. Technical Report Deliverable D5.1, ECC-SMART, 2022.

[70] J. Duspiva, G. Mazzini, J. Čada, M. Šípová, A. Prošek, L. Cizelj, A. Kiss, I. Boros, S. Czifrus, A. Saéz Maderuelo, O. Martin, and R. Novotný. D5.4 guidelines for the demonstration of the safety of the scw-smr concept. Technical Report Deliverable D5.4, ECC-SMART, 2024.

[71] A. Prošek and L. Cizelj. D5.3 pre-licensing study. Technical Report Deliverable D5.3, ECC-SMART, 2024.

A Pre-Conceptual Design Requirements

The pre-conceptual design requirements for the European SCW-SMR have been established through an iterative process involving all technical disciplines within the ECC-SMART project. The pre-conceptual design requirements are summarized in the table 10.

The design must also satisfy requirements for criticality control and inherent safety:

- **Reactivity feedback coefficients**:
  - Coolant temperature: -16.8±1.6 pcm/K (MOX), -23.1±0.7 pcm/K (UO_2)
  - Moderator temperature: -10.6±0.5 pcm/K (MOX), -5.5±0.4 pcm/K (UO_2)
  - Fuel temperature: -1.27±0.17 pcm/K
- **Shutdown capability**: Minimum 2000 pcm margin with N-1 criterion
- **Power distribution limits**: Ensure adequate safety margins throughout cycle

B Detailed Design Parameters

The table 11 provide detailed parameter summary of the European SCW-SMR.

Table 10: Design requirements for the European SCW-SMR

Parameter	**Value/Range**
Thermal power	290 MW_{th}
Electric power	∼128 MW_e
System pressure	25 MPa
Core inlet temperature	280°C
Core outlet temperature	500-520°C
Maximum cladding temperature (normal)	<625°C
Maximum cladding temperature (DBA)	<850°C
Peak linear heat rate	≤39 kW/m
Fuel enrichment	<20% U-235
Fuel burnup	>40 GWd/tHM
Design lifetime	60 years
Capacity factor	>90%
Refueling interval	18-24 months
Construction time	<4 years

Table 11: Design parameters for EU SCW-SMR

Parameter	**Unit**	**Value**
Fuel Pin Geometry		
Fuel rod outer diameter	m	0.008
Fuel gas gap thickness	m	0.00005
Fuel cladding thickness	m	0.0005
Fuel rod wire spacer diameter	m	0.00134
Fuel rod wire spacer axial pitch	m	0.2
Fuel heated length per heat-up stage	m	1.68
Fuel Pin Materials and Properties		
Fuel enrichment	-	Variable
Fuel density	kg/m^3	11,000
Fuel conductivity	W/m/K	Built-in UO2
Fuel specific heat capacity	J/kg/K	Built-in UO2
Fuel gas gap material	-	Helium
Fuel gas gap conductivity	W/m/K	0.7193
Fuel cladding material	-	310S
Fuel Assembly Geometry		
Pin number per assembly	-	40
Fuel rod pitch	m	0.00944
Assembly box inner width	m	0.0675
Assembly box wall thickness	m	0.0069
Moderator box inner width	m	0.0205
Moderator box wall thickness	m	0.0032

(continued on next page)

(continued from previous page)

Parameter	Unit	Value
Total coolant flow path length	m	1.985
Assembly Materials		
Assembly box inner liner material	-	310S
Assembly box insulation material	-	YSZ
Assembly box outer liner material	-	Zircaloy-4
Insulation thermal conductivity	W/m/K	2.0
Reactor Core Geometry		
Number of fuel assemblies	-	400
Fuel assembly pitch	m	0.0993
Lattice type	-	Square
RPV inner width	m	4.17
RPV wall thickness	m	0.25
Reactor total height	m	8.1
Operating Conditions		
Core thermal power	MW	290
Operating pressure	MPa	25
Core inlet temperature	°C	280
Core outlet temperature	°C	500
Mass flow rate	kg/s	144-150
Peak linear power rating	kW/m	39
Reactivity Coefficients		
Coolant temperature coefficient	pcm/K	-16.8 ± 1.6
Moderator temperature coefficient	pcm/K	-10.6 ± 0.5
Fuel temperature coefficient	pcm/K	-1.3 ± 0.2